Unexpected inhibition of motor function by dopamine activation of D1/D2 co-expressing striatal neurons.

Authors:

Patricia Bonnavion[1,†], Christophe Varin[1,†], Ghazal Fakhfouri[2], Aurélie De Groote[1], Amandine Cornil[1], Elsa Isingrini[2,3], Quentin Rainer[2] , Kathleen Xu[2], Eleni Tzavara[3,4], Erika Vigneault[2], Sylvie Dumas[5], Alban de Kerchove d'Exaerde[1,‡*] and Bruno Giros[2,3,‡*]

Affiliations:

[1]Université Libre Bruxelles (ULB), ULB Neurosci Inst, Neurophy Lab; Brussels, Belgium.
[2]Department of Psychiatry, Douglas Hospital, Mc Gill University; Montreal, QC, Canada.
[3]Université de Paris, INCC UMR 8002, CNRS ; F-75006 Paris, France.
[4] AP-HM, Hôpital Sainte Marguerite, Pôle Psychiatrie Universitaire Solaris ; Marseille, France
[5]Oramacell; 75006 Paris, France
†These authors contributed equally to this work
‡Equal senior contribution
*Correspondence to BG (bruno.giros@mcgill.ca) or AKE (adekerch@ulb.ac.be)

Abstract:

The central function of the striatum and its dopaminergic (DA) afference in motor control and integration of cognitive and emotional processes is commonly explained by the two striatal efferent pathways characterized by striatal projection neurons (SPNs) expressing DA D1 receptor- and D2 receptor (D1-SPNs and D2-SPNs), respectively, regardless of SPNs co-expressing these two receptors (D1/D2-SPNs). Here, after developing an approach that enables to target these hybrid SPNs, we demonstrated that, although these SPNs are rare, they play a major role in guiding the motor function of the other two main populations and convey a DA-mediated antagonistic motor brake. D1/D2-SPNs project exclusively to the external globus pallidus (GPe) and have specific electrophysiological features with distinctive integration of DA signals. Optogenetic stimulation and loss-of-function experiments indicated that D1/D2-SPNs potentiate the prokinetic and antikinetic functions of D1-SPNs and D2-SPNs, respectively, and restrain the integrated motor response to psychostimulants. Overall, our findings demonstrate the essential role of this third unacknowledged population of D1/D2 co-expressing neurons, which orchestrates the fine-tuning of DA regulation in the thalamo-cortico-striatal loops.

One-Sentence Summary:

D1/D2 striatal output promotes dopamine-induced motor inhibition

Main text

The thalamo-cortico-striatal loops are essential cerebral modules for initiation, integration and regulation of motor, cognitive and emotional processes[1-4.] The functional specificity and precision of their actions are finely tuned through the complex design of the striatal organization[5-7]. Striatal control of cortical excitation and inhibition requires two distinct output pathways[8,9]: a direct pathway (cortex→striatum→GPi/SNr) facilitates motor cortical activity, whereas an indirect pathway (cortex→striatum→GPe→STN→GPi/SNr) inhibits motor cortex. The direct pathway involves Striatal Projection Neurons (SPNs) expressing the DA D1 receptor (D1R), while the indirect pathway involves SPNs expressing the dopamine D2 receptor (D2R)[10]. This organization substantiates why DA is such an essential neurotransmitter in movement and motor control[11] but also in the reward system and cognitive processes[12]. Because DA stimulates D1-SPNs in the direct pathway and inhibits D2-SPNs in the indirect pathway, it has a synergistic effect promoting locomotion. Consistently, the motor response to cocaine administration is suppressed or blunted in D1R-KO[13] and SPNs-D2R KO[14], respectively. Despite these effects attributing a unique and homogeneous role to DA in the striatum, growing evidence indicates several levels of heterogeneity within the rodent striatal system that still poorly integrate the striatal actions of DA. In contrast to the classical model suggesting opposite motor roles of the two SPNs populations, it has been shown that optogenetic activation of D1- and D2-SPNs produces different responses in SNr and cortical neurons, with stimulation of each pathway eliciting both excitations and inhibitions[15-17]. Moreover, it has been also shown that both populations are jointly active during a motor task[18-21]. Finally, single-cell molecular analysis of striatal neurons reveals more complex heterogeneity and identifies several distinct clusters of SPNs[22-27]. Notably, in addition to the presence of D1-SPNs and D2-SPNs, the existence of hybrid SPNs co-expressing D1R and D2R has been described, which had previously been identified by indirect approaches[28-32] but whose role and functions remain unknown. Using targeted approaches, we demonstrate here that this population of hybrid D1/D2-SPNs gives rise to a third specific efferent pathway with critical functions for motor control and its DA-mediated modulation in an organized combination with the two canonical D1- and D2-SPNs pathways.

SPNs co-expressing D1/D2 constitute a specific population.

Previous single-cell and transgenic studies have provided only indirect and sometimes controversial indications of D1/D2-SPNs distribution[28-32]. Here we used direct and highly sensitive double-probe *in situ* hybridization (sdFISH) throughout the striatum to demonstrate native co-expression of D1R and D2R. Unbiased automated quantitative analysis showed that D1R/D2R co-expressing cells accounted for 6-7% of all cells (expressing D1R and D2R) in both the dorsal and ventral parts of the striatum, across its rostro-caudal extent (Fig. **1a-b**, Extended Data Fig. **1a,b**).

To selectively target this population of SPNs co-expressing D1R and D2R, we used an intersectional approach[33] (Fig. **1c**) by generating a novel $D1^{FlpO}$ driver line expressing Flp recombinase (FlpO) in D1-SPNs (Extended Data Fig. **1c-d**). $D1^{FlpO}$ were crossed with the $A2a^{Cre}$ driver line expressing Cre recombinase exclusively in D2-SPNs, thereby excluding cholinergic interneurons[34] (Extended Data Fig. **1e**). Using this approach, we were able to individually target for the first time SPNs expressing both D1R and D2R (D1/D2-SPNs), but to also access and control SPNs exclusively expressing D1R (D1-SPNs) and SPNs exclusively expressing D2R (D2-SPNs). This relies upon the presence of Cre (C) and/or FlpO (F): **C**on/**F**on, **C**off/**F**on and **C**on/**F**off, respectively (Fig.**1c**). We first used channel rhodopsin 2 (ChR2) expression with INTRSECT

vectors to trace neuronal pathways. We found that D1/D2-SPNs have a single projection pathway to the external globus pallidus (GPe), dissociating them from a direct pathway to the internal globus pallidus (GPi)/substantia nigra pars reticulata (SNr) (Fig. **1d**). This mapping highlights that D1/D2-SPNs give rise to an additional indirect pathway as D2-SPNs, which may therefore mediate reverse effects of DA on the thalamo-cortical loop through D1R activation. Furthermore, with respect to their cell morphology, this population is distinguished by a more ramified proximal arborization than D1-SPNs and a larger soma area than D2-SPNs (Fig. **1e-g**), suggesting that these D1/D2 co-expressing neurons may have distinct physiological properties and carry different functions than D1-SPNs and D2-SPNs.

D1/D2-SPNs display exclusive electrophysiological features.

Based on their morphological specificity, we hypothesized additional distinctions and we examined the electrophysiological properties of D1/D2-SPNs in comparison with the two classical populations. Thirty electrophysiological parameters were extracted from whole-cell current clamp recordings describing passive membrane properties, firing properties, action potentials properties and threshold properties (Fig. **2a-c,** Extended Data Table **1**). As previously reported[35-37], D1- and D2-SPNs differed with respect to many features (Fig. **2c-k,** Extended Data Fig. **2a-c**). We found some mixed properties for the D1/D2-SPNs, the intensity to saturation and the current frequency early slope are similar to those of D1-SPNs (Fig. **2h-i**) while the step intensity to first action potential is similar to D2-SPNs (Fig. **2g,** Extended Data Table **1**). More essentially, D1/D2-SPNs exhibit exclusive action potential properties such as lower AP threshold and larger AP amplitude (Fig. **2e,j-k,** Extended Data Fig. **2**). Taking together, anatomical, morphological and electrophysiological results substantiate the reality of a third functional SPNs population.

D1/D2-SPNs selectively control the locomotor brake.

To identify the motor function of this third SPN population, we performed in vivo optogenetic stimulations of D1/D2-SPNs in the dorsomedial part of the striatum (Fig. **3**, Extended Data Fig. **3**). Unilateral activation of the indirect pathway has been shown to mimic ipsiversive rotational behavior, whereas activation of the direct pathway results in contraversive rotations[38]. Consistent with their GPe-targeted projection pattern, unilateral stimulation of D1/D2-SPNs also results in ipsilateral rotations, like that of D2-SPNs while stimulation of D1-SPNs results in the opposite rotatory behavior (Fig. **3b**). These effects directly validate that our intersectional optogenetic strategy is effective in all three populations. We next examined the impact of D1/D2-SPNs stimulation on free-running mice in an open field test (Fig. **3c-f**, Extended Data Fig. **4,5**). Motor behavior was classified into three states: locomotion, small movements, and immobility. Remarkably, activation of this minority of D1/D2-SPNs significantly impedes locomotion by reducing total time spent in this ambulatory motor state. In addition, optogenetic stimulation of D1- and D2-SPNs induces no effect on locomotion (Fig. **3c**, Extended Data Fig. **4a-c**). It contrasts with previous optogenetic experiments using stimulation of direct or indirect pathway SPNs intermixed with D1/D2-SPNs[5]. Apart from this intriguing difference in locomotion, D1/D2-SPNs activation does everything one would expect from an indirect pathway, such as the D2-SPNs. Indeed, we observe an increase and consolidation of the state of immobility by lengthening the duration of immobility episodes and increasing the probability of remaining in this state (Extended Data Fig. **4c,5**). Concomitantly, small movements are strongly inhibited as observed with a stimulation of D2-SPNs. In contrast, the activation of D1-SPNs increases small movements at the

expense of immobility. To refine examination of the locomotion state, which remains prominently expressed before and during stimulations (Fig. **3d**), we checked the velocity profile and accelerations around the onset of locomotion (Fig. **3e-f**, Extended Data Fig. **4d-f**). Stimulation of D1/D2-SPNs, as well as D2-SPNs, increases both velocity and acceleration when animals engage in locomotion. Conversely, D1-SPNs stimulation elicited a slowing of locomotor state with lower speeds and accelerations. These responses may be driven by behavior triggered by the aversive or rewarding effects of indirect or direct pathway activation, respectively[39,40]. Overall, these results reveal highly effective and specific control of D1/D2-SPNs over locomotion, revising the simplistic bimodal prokinetic and antikinetic roles of SPNs outputs exclusive to D1R and D2R.

D1/D2-SPNs catalyze to the functional identity of other SPNs.

Comparison of the populations of "mixed" SPNs (D1+D1/D2 and D2+D1/D2), as studied so far and in which there is co-activation of D1/D2-SPNs, and "exclusive" D1- and D2-SPNs, excluding the hybrid D1/D2 population, allows to obtain additional information on the functional role of D1/D2-SPNs, but also to re-examine the respective roles of D1- and D2-SPNs. We examined the kinetics of motor state change around each optogenetic stimulation event: before, immediately at the onset of stimulation (early stim), at the end of the stimulation period (late stim), and after stimulation (10 trials per mouse; Fig.**4a-b**).

These analyses first reveal major differences between exclusive D1-SPNs and mixed D1+D1/D2-SPNs in response to stimulation (Fig. **4a1-a2, b**). Immediately at the onset of stimulation (Fig. **4a1-a2, b**), exclusive and mixed D1-SPNs induce the same response, namely a transient decrease in locomotion with a concomitant increase in small movements. Furthermore, these immediate effects are not yet associated with inhibition of immobility, which appears later during stimulation (Fig. **4b**). The contrasting difference between D1 and D1+D1/D2-SPNs occurs late in the course of stimulation, showing a strong increase in locomotion and inhibition of small movements only when D1/D2-SPNs are co-activated (Fig. **4b**). These locomotion-promoting effects during simultaneous stimulation of D1- and D1/D2-SPNs are consistent with the stabilization of the locomotor state underpinned by a lengthening of locomotor episodes, not observed in stimulation of exclusive D1-SPNs (Extended Data Fig. **4a**). On the contrary, “exclusive” D1-SPNs stimulation results mainly on the induction of small movements, which is prevented by the co-stimulation of D1/D2-SPNs (Extended Data Fig. **4b**). To extend this characterization of motor state changes, we applied a Markov chain model to assess how the dynamic organization of motor states is affected by each SPNs stimulation (Fig. **4c,** Extended Data Fig. **5**). Conditional transition probabilities highlight that activation of D1-SPNs alone facilitates small movements by inhibiting exit probabilities from this state and increasing entry probabilities from immobility. Conversely, this convergence to small movements is less strong when D1-SPNs are co-activated with D1/D2-SPNs because transitions from small movements to locomotion persist while reciprocal transitions from locomotion to small movements are inhibited (Fig. **4c**, Extended Fig. **5**). Altogether, these findings indicate that activation of D1/D2-SPNs is required to trigger the prokinetic effects associated with activation of the classical direct pathway.

These comparative analyses also identified differences in the exclusive and mixed D2-SPNs populations, illustrated by a divergence of effects on state changes to the locomotor state depending on whether D1/D2-SPNs are co-activated or not (Fig. **4a3-a4, b**). Throughout the duration of stimulation, the probability of being in the locomotor state is increased under exclusive D2-SPNs stimulation (Fig. **4a3,b**), and this is prevented by co-stimulation with D1/D2-SPNs (Fig.

4a4,b). Consistently, computing conditional transition probabilities under D2-SPNs and D1/D2+D2-SPNs activations indicates an increased probability of remaining in locomotor state and increased entries into locomotion from immobility, both observed only under stimulation of D2-SPNs (Fig. **4c**, Extended Data Fig. **5**). These results indicate that co-activation of D1/D2-SPNs alongside D2-SPNs blocks the prokinetic effects induced by exclusive stimulation of D2-SPNs and thus further facilitates the antikinetic role of the indirect pathway activation.

Dopamine exerts a unique effect on D1/D2-SPNs activity.

Given the fundamental role of DA on locomotion in the striatum, we explored its actions and functions on these hybrid SPNs. We first evaluated ex vivo the effects of DA bath application on SPNs activity (Fig. **5**, Extended Data Fig. **6**). We confirmed that, at depolarized membrane potentials, DA depolarizes D1-SPNs whereas it hyperpolarizes D2-SPNs (Fig. **5c,** Extended Data Fig. **6b**). Consistently, it increases D1-SPNs excitability and decreases D2-SPNs excitability, as indicated by substantial changes in firing response to depolarizing current pulses, membrane resistance, and the current-frequency relationship (Fig. **5d-e**, Extended Data Fig. **6c-e**). In addition, with respect to AP properties, we also confirmed a decrease in AP threshold in both population in response to DA (Fig. **5f**), and ramp current to AP threshold is significantly decreased in D1-SPNs whereas it is unchanged in D2-SPNs (Fig. **5g**).

For D1/D2-SPNs, we found a DA-induced depolarization in a D1R activation-dependent manner (Fig. **5a-c**, Extended Data Fig. **6c,h**), but no change in excitability or firing (Fig. **5d-e**, Extended Data Fig. **6a-e**). This lack of effect might be related to the peculiar D1/D2-SPN AP properties previously described (Fig. **2**). Indeed, in sharp contrast to the two other SPNs populations, we observed that DA increases the AP threshold in D1/D2-SPNs (Fig. **5b,f**), which is abolished in the presence of either D1R or D2R antagonists (Extended Data Fig. **6k-m**). In addition, the ramp current to AP threshold is unchanged (**Fig. 5g**). These observations reinforce the singularity of D1/D2-SPNs that distinctly integrate DA signals, potentially in a manner mediated by the coactivation of D1R and D2R.

Loss of D1/D2 co-expression impairs in vivo DA response

To highlight the importance of the integration of DA signaling in D1/D2-SPNs *in vivo*, we generated a model in which the D1R gene was deleted selectively in D2-SPNs ($D1^{cKO}$/D2 mice). As a result, the $D1^{cKO}$/D2 mice have a true engineered two striatal output pathway system, with direct D1-SPNs output and one single indirect striatal output with all neurons only expressing D2R (Fig. **6a-b**). In this model, the D1/D2 output is therefore suppressed.

To evaluate the integrated responsiveness of $D1^{cKO}$/D2 mice under DA stimulation, we examined motor responses to different doses of cocaine in the open field. Our first observations show a greater sensitivity to low doses of cocaine in $D1^{cKO}$/D2 mice (Fig. **6c-d**). Conversely, no difference is observed for the highest dose tested (Fig. **6c-d**). The latter effects were also observed with amphetamine treatment (Extended Data Fig. **7a**). Moreover, the temporal integration of the cocaine response differs between $D1^{cKO}$/D2 mice and controls. Indeed, the peak effect of cocaine appears shortly after its administration in control mice whereas it is delayed in $D1^{cKO}$/D2 mice, indicating a slowing of the temporal integration of DA signals in mice devoid of D1/D2 co-expression.

In addition to the acute effect, we probed chronic integration of DA signal by repeated exposure to cocaine (Fig. **6e**). Strikingly, daily cocaine administration does not trigger an increase in

locomotion in D1^{cKO}/D2 mice, as observed in control animals (Fig. **6e**, Extended Data Fig. **7b**). The locomotor response showed a similar time course as the response to acute administration (Extended Data Fig. **7b**). These findings demonstrate that co-expression of D1R/D2R is required for motor responses to enhanced DA neurotransmission. Noteworthy, spatial integration of cocaine-cued reward is not affected, as cocaine place preference is maintained in both D1^{cKO}/D2 mice and controls (Fig. **6f**), indicating that the phenotype we observe engages motor circuits rather than reward-related pathways. Consistently, D1^{cKO}/D2 mice exhibit motor impairments marked by increased locomotion, as illustrated in saline conditions of drug dose-responses (Fig. **6c**, Extended Fig. **7a**). Altogether, these observations highlight an essential role for D1/D2-SPNs in the integration of DA signals and in the functioning of the striatum, which could not operate properly with only two efferent pathways.

Discussion

Our findings demonstrate that the striatum computes and relays information through three efferent pathways. We highlighted a third population of SPNs in the striatum that is distinguished by co-expression of D1R and D2R and that projects specifically to the GPe. These neurons may partially account for the described genetic heterogeneity of SPNs[22-27]. Accordingly, further functional subdivisions between SPN subtypes may arise by taking into consideration the existence of genetic distinction between SPNs located in the matrix or in striosomes, or located in the medial or lateral subdivisions of the dorsal striatum[22-23]. These additional subtypes would likely display unique properties such as their input-output connectivity, or their integration of various neurotransmitter signals that should be linked with specific functions during defined behaviors. Thanks to the comprehensive characterization of genetic markers expressed by SPNs[22-27], addressing these issues could be achieved using combination of multiple genetic markers like we did in this study with two-factor intersectional tools. This approach could also be enhanced using three-factor intersectional methods[41].

Our optogenetic studies revealed that D1/D2-SPNs provide key control over the global functioning of the dorsal striatum to control appropriate transitions between motor states. We showed that only the stimulation of these neurons was responsible for inducing a brake on locomotion. We observed that D1/D2-SPNs, when coactivated with D1- or D2-SPNs, act as conductors of striatal locomotion and shape the functional identity of D1- and D2-SPNs as described so far, i.e. pro- and antikinetic, respectively. Our study also revealed new effects of D1- and D2-SPNs excitations on motor states, which differ from a bidirectional control on locomotion, namely a locked state in the promotion of small "parasite" movements under D1-SPNs activation, or locomotor initiations by error under D2-SPNs activation. Most importantly, disruption of this pathway, which comprises 6-7% of all SPNs, has major functional consequences for spontaneous behavior and integration of DA signals. The striking difference in psychostimulant effects in D1^{cKO}/D2 mice clearly demonstrates that under normal conditions, DA activation of the D1R in hybrid D1/D2-SPNs has opposite effects to D2R stimulation of indirect D2-SPNs in inhibiting locomotion. In the D1^{cKO}/D2 mice, this motor inhibition could no longer be effective, and the effects of cocaine are enhanced (or no longer buffered). This is a direct consequence of their unique electrophysiological properties. Indeed, although D1/D2-SPNs displayed a DA-induced depolarization following D1R activation, their firing rate remained unchanged. Therefore, upon glutamate activation by cortico-striatal and thalamo-striatal principal neurons, and in contrast to D2-SPNs that are inhibited by DA[42], D1/D2-SPNs will convey an activation of the indirect pathway resulting in motor inhibition. Consequently, D1/D2-SPNs maintain a necessary homeostatic balance between the direct and

indirect pathways to prevent DA-mediated convergent activation of the basal ganglia output nuclei leading to overactivation of the thalamo-cortical systems (Extended Data **Fig. 8**). We therefore propose that D1/D2-SPNs provide a key balance necessary for proper striatal functioning. This balance between D1/D2-, D1-, and D2-SPNs is likely formed during embryonic stages and matures during early postnatal development, following a stage where more SPNs co-express both D1R and D2R[43-45]. Only a fraction of SPNs in the indirect pathway will conserve expression of both D1R and D2R, whereas most express only D2R, and all SPNs in the direct pathway express only D1R. It remains to be determined how these less abundant D1/D2-SPNs interact with and integrate into the other two SPNs populations in different areas of the striatum during more elaborate striatal-dependent behaviors[46].

Improper establishment of this balance or its subsequent dysregulation could lie at the core of certain neurophysiological disorders involving a dysregulation of striatal function. For example, the positive symptoms of schizophrenia are related to a hyperdopaminergic state in the mesolimbic system[47] and in particular in the dorsal striatum[48]. Thus, abnormal coordination of the three striatal output pathways, and in particular the one formed by D1/D2-SPNs, could be an unsuspected susceptibility risk for psychiatric disorders, as well as its involvement in motor control in neurological disorders such as Parkinson's disease.

References:

1. H.l. Groenewegen , H. W. Berendse, Anatomical Relationships Between the Prefrontal Cortex and the Basal Ganglia in the Rat. in *Motor and Cognitive Functions' of the Prefrontal Cortex*, A.-M. Thierry, J. Glowinski ,P.S. Goldman-Rakic ,Y. Christen Eds, Springer-Verlag Berlin Heidelberg , 51-77 (1994).
2. D. Joel and I. Weiner, The connections of the primate subthalamic nucleus: indirect pathways and the open-interconnected scheme of basal ganglia-thalamocortical circuitry, *Brain Research Reviews* **23**, 62–78 (1997)
3. M.W. Shiflett and B.W. Balleine, Molecular substrates of action control in cortico-striatal circuits. *Progress in Neurobiology* **95,** 1–13 (2011).
4. M. Jahanshahi et al., A fronto–striato–subthalamic–pallidal network for goal-directed and habitual inhibition. *Nature Rev. Neurosci*.**16**, 719-732 (2015).
5. P. Bolam et al., Synaptic organisation of the basal ganglia. *J. Anat.* **196**, 527-542 (2000).
6. A. C. Kreitzer and R. C. Malenka, Striatal Plasticity and Basal Ganglia Circuit Function. *Neuron* **26**, 543-554 (2008).
7. H. Schroll and F. H. Hamker, Computational models of basal-ganglia pathway functions: focus on functional neuroanatomy. *Frontiers Syst. Neurosci.* **7**, 122 (2013).
8. R. L. Albin, A. B. Young, J. B. Penney, The functional anatomy of basal ganglia disorders. *Trends Neurosci*, **12**, 366-375 (1989).
9. M. R. DeLong, Primate models of Movment disorder of basal ganglia origin. *Trends Neurosci.* **13**, 281-285 (1990).
10. C. R. Gerfen *et al.*, D1 and D2 dopamine receptor-regulated gene expression of striatonigral and striatopallidal neurons. *Science* **250**, 1429-1432 (1990).
11. S. Cataldi *et al.*, Interpreting the role of the striatum during multiple phase of motor learning *FEBS J.* 0.1111/febs.15908 (2021).

12. L. A. Gunaydin, A. C. Kreitzer, Cortico-Basal Ganglia Circuit Function in Psychiatric Disease. *Annu Rev Physiol* **78**, 327-350 (2016).
13. M. Xu *et al.*, Elimination of cocaine-induced hyperactivity and dopamine-mediated neurophysiological effects in dopamine D1 receptor mutant mice. *Cell*. **79**, 945-955 (1994).
14. G. Kharkwal *et al.*, Dopamine D2 receptors in striatal output neurons enable the psychomotor effects of cocaine. *Proc Natl Acad Sci U S ,* **113**, 11609-11614 (2016).
15. B.S. Freeze, A.V. Kravitz, N. Hammack, J.D. Berke, A.C. Kreitzer, Control of basal ganglia output by direct and indirect pathways projection neurons *Journal of neuroscience : the official journal of the Society for Neuroscience* **33**, 18531-18539 (2013)
16. I. A. Oldenburg, B.L. Sabatini, Antagonistic but not symmetric regulation of primary motor cortex by basal gangli direct and indirect pathways. *Neuron* **86**,1174-1181 (2015).
17. H.J. Lee *et al.*, Activation of Direct and Indirect Pathway Medium Spiny Neurons Drives Distinct Brain-wide Responses. *Neuron* **91**, 412-424 (2016).
18. G. Cui *et al.*, Concurrent activation of striatal direct and indirect pathways during action initiation. *Nature* **494**, 238-242 (2013).
19. E. A. Yttri, J. T. Dudman, Opponent and bidirectional control of movment velocity in the basal ganglia. *Nature* **533**, 402-406 (2016).
20. A. Klaus *et al.*, The spatiotemporal organization of the striatum encodes action space. *Neuron* **96**, 1171-1180 (2017).
21. J. G. Parker *et al.* , Diametric neural ensemble dynamics in parkinsonian and dyskinetic states. *Nature* **557**, 177-182 (2018).
22. O. Gokce *et al.*, Cellular Taxonomy of the Mouse Striatum as Revealed by Single-Cell RNA-Seq. *Cell Rep* **16**, 1126-1137 (2016).
23. A. Martin *et al.*, A Spatiomolecular Map of the Striatum. *Cell Rep* **29**, 4320-4333 e4325 (2019).
24 . A. Saunders *et al.*, Molecular Diversity and Specializations among the Cells of the Adult Mouse Brain. *Cell* **174**, 1015-1030 e1016 (2018).
25. G. Stanley, O. Gokce, R. C. Malenka, T. C. Sudhof, S. R. Quake, Continuous and Discrete Neuron Types of the Adult Murine Striatum. *Neuron* **105**, 688-699 e688 (2020).
26. X. Xiao *et al.*, A Genetically Defined Compartmentalized Striatal Direct Pathway for Negative Reinforcement. *Cell* **183**, 211-227 e220 (2020).
27. A. Zeisel *et al.*, Molecular Architecture of the Mouse Nervous System. *Cell* **174**, 999-1014 e1022 (2018).
28. O. Aizman *et al.*, Anatomical and physiological evidence for D1 and D2 dopamine receptor colocalization in neostriatal neurons. *Nature neuroscience* **3**, 226-230 (2000).
29. J. Bertran-Gonzalez *et al.*, Opposing patterns of signaling activation in dopamine D1 and D2 receptor-expressing striatal neurons in response to cocaine and haloperidol. *The Journal of neuroscience : the official journal of the Society for Neuroscience* **28**, 5671-5685 (2008).
30. M. Matamales *et al.*, Striatal medium-sized spiny neurons: identification by nuclear staining and study of neuronal subpopulations in BAC transgenic mice. *PloS one* **4**, e4770 (2009).
31. J. A. Shuen, M. Chen, B. Gloss, N. Calakos, Drd1a-tdTomato BAC transgenic mice for simultaneous visualization of medium spiny neurons in the direct and indirect pathways of the basal ganglia. *The Journal of neuroscience : the official journal of the Society for Neuroscience* **28**, 2681-2685 (2008).
32. D. Thibault, F. Loustalot, G. M. Fortin, M. J. Bourque, L. E. Trudeau, Evaluation of D1 and D2 dopamine receptor segregation in the developing striatum using BAC transgenic mice. *PloS one* **8**, e67219 (2013).

33. L. E. Fenno *et al.*, Targeting cells with single vectors using multiple-feature Boolean logic. *Nature methods* **11**, 763-772 (2014).
34. P. F. Durieux *et al.*, D2R striatopallidal neurons inhibit both locomotor and drug reward processes. *Nat Neurosci* **12**, 393-395 (2009).
35. C. Cepeda *et al.*, Differential electrophysiological properties of dopamine D1 and D2 receptor-containing striatal medium-sized spiny neurons. *The European journal of neuroscience* **27**, 671-682 (2008).
36. T. S. Gertler, C. S. Chan, D. J. Surmeier, Dichotomous anatomical properties of adult striatal medium spiny neurons. *The Journal of neuroscience : the official journal of the Society for Neuroscience* **28**, 10814-10824 (2008).
37. H. Planert, T. K. Berger, G. Silberberg, Membrane properties of striatal direct and indirect pathway neurons in mouse and rat slices and their modulation by dopamine. *PloS one* **8**, e57054 (2013).
38. A. V. Kravitz *et al.*, Regulation of parkinsonian motor behaviours by optogenetic control of basal ganglia circuitry. *Nature* **466**, 622-626 (2010).
39. T. Hikida *et al.*, Distinct roles of synaptic transmission in direct and indirect straital pathways to reward and aversive behavior. *Neuron* **66**, 896-907 (2010).
40. A.V. Kravitz, L. D. Tye, A. C. Kreitzer, Distinct roles for direct and indirect pathway striat neurons in reinforcement. *Nat Neurosci* **15**, 816-818 (2012).
41. L.E. Fenno *et al.*, Comprehensive Dual- and Triple-Feature Intersectional Single-Vector Delivery of Diverse Functional Payloads to Cells of Behaving Mammals. *Neuron* **107**, 836-853 (2020).
42. G. E. Alexander, M. D. Crutcher, Preparation of movment: neural representations of intended direction in three motor areas of the monkey. *Trends Neurosci*, **13**, 266-271 (1990).
43. Biezonski *et al.*, Evidence for limited D1 and D2 receptor coexpression and colocalization within the dorsal striatum of the neonatal mouse. *J Comp Neurol* **523**, 1175-1189 (2015).
44. S.M. Kelly *et al.,* Radial Glial Lineage Progression and Differential Intermediate Progenitor Amplification Underlie Striatal Compartments and Circuit Organization. *Neuron* **99**,345-361 (2018).
45. A. Tinterri *et al*., Active intermixing of indirect and direct neurons builds the striatal mosaic. *Nat Commun* **9**, 4725 (2018).
46. M. Matamales *et al.*, Local D2- to D1-neuron transmodulation updates goal-directed learning in the striatum. *Science* **367**, 549-555 (2020).
47. O.D. Howes and S. Kapur, The dopamine hypothesis of schizophrenia: version III--the final common pathway. *Schizophr Bull.* **35,** 549-562 (2009).
48. H. Sekiguchi, G. Pavey, and B. Dean, Altered levels of dopamine transporter in the frontal pole and dorsal striatum in schizophrenia. *NPJ Schizophr* **5**, 20 (2019).

Supplemental references:

49. S. Dumas, Å. Wallén-Mackenzie, Developmental Co-expression of Vglut2 and Nurr1 in a Mes-Di-Encephalic Continuum Preceeds Dopamine and Glutamate Neuron Specification. *Front Cell Dev Biol*. **7**, 307 (2019).
50. A. H. Hopman, F. C. Ramaekers, E. J. Speel, Rapid synthesis of biotin-, digoxigenin-, trinitrophenyl-, and fluorochrome-labeled tyramides and their application for In situ hybridization using CARD amplification. *J Histochem Cytochem*. **46**, 771–777 (1998).

51. A. E. Carpenter *et al.*, CellProfiler: image analysis software for identifying and quantifying cell phenotypes. *Genome Biol*. **7**, R100 (2006).
52. Y. Kawaguchi, C. J. Wilson, P. C. Emson, Intracellular recording of identified neostriatal patch and matrix spiny cells in a slice preparation preserving cortical inputs. *J Neurophysiol*. **62**, 1052–1068 (1989).
53. Petilla Interneuron Nomenclature Group, G. A. Ascoli, *et al.*, Petilla terminology: nomenclature of features of GABAergic interneurons of the cerebral cortex. *Nat Rev Neurosci*. **9**, 557–568 (2008).
54. B. Halabisky, F. Shen, J. R. Huguenard, D. A. Prince, Electrophysiological classification of somatostatin-positive interneurons in mouse sensorimotor cortex. *J Neurophysiol*. **96**, 834–845 (2006).
55. C. L. Cunningham, S. D. Dickinson, N. J. Grahame, D. M. Okorn, C. S. McMullin, Genetic differences in cocaine-induced conditioned place preference in mice depend on conditioning trial duration. *Psychopharmacology (Berl)*. **146**, 73–80 (1999).

Acknowledgments: We thank Marc G Caron, Ami Citri, Philippe Faure, Christophe Kellendonk, Christian Lüsher, Marina Piciotto, Gilad Silberberg and Laurent Venance for critical reading of the manuscript. We thank Charu Ramakrishnan and Karl Deisseroth for providing additional Intrsect viruses. We thank Delphine Houtteman, Souad Laghmari, Perrine Hagué and Laetitia Cuvelier for technical assistance and mice colonies in Brussels, Yeqing Geng for taking care of the mice colonies in Montréal and Stéphanie De Gois for assistance in imaging techniques. PB is a research associate of FRS-FNRS (Belgium). CV is a postdoctoral researcher of FRS-FNRS (Belgium), GF is a postdoctoral researcher of FRQS (Canada). ADG and AC are research fellows of FRS-FNRS (Belgium). AKE is a Research Director of the FRS-FNRS. BG is a Canada Research Chair and a visiting professor at Université de Paris.

Funding: This work was supported by grants from the Canadian Institute for Health Research (201803PJT-399980-PT) and the Graham Boeckh Foundation to BG; from FRS-FNRS (#23587797, #33659288, #33659296), Welbio (#30256053), Fondation Simone et Pierre Clerdent (Prize 2018) and Fondation ULB to AKE; from FRS-FNRS (#34793348, #35285205) to PB.

Author contributions: Conceptualization: BG, PB and AKE; Investigation for optogenetic experiments: PB; Methodology and investigation for motor analysis: PB, CV with the support of AC; Methodology and investigation for electrophysiological experiments: CV; Investigation for 3D reconstruction: ADG; Investigation for behavioral experiments on $D1^{cKO}$/D2: GF, QR with the support of KX, EI and PB; Investigation for the FISH experiments: SD with the support of AC; Supervision for the animal colonies: EV; Resources for the D1flpO strain: ET; Formal analysis: PB, CV, AC, BG and AKE; Validation and supervision: PB, BG and AKE; Writing: PB, CV, AKE and BG.

Competing interests: The authors declare no competing interests. **Data and materials availability:** All data are available in the manuscript or the supplementary materials. The three transgenic mice strains will be shared after completion of a MTA to prevent conflict of interest on research subjects.

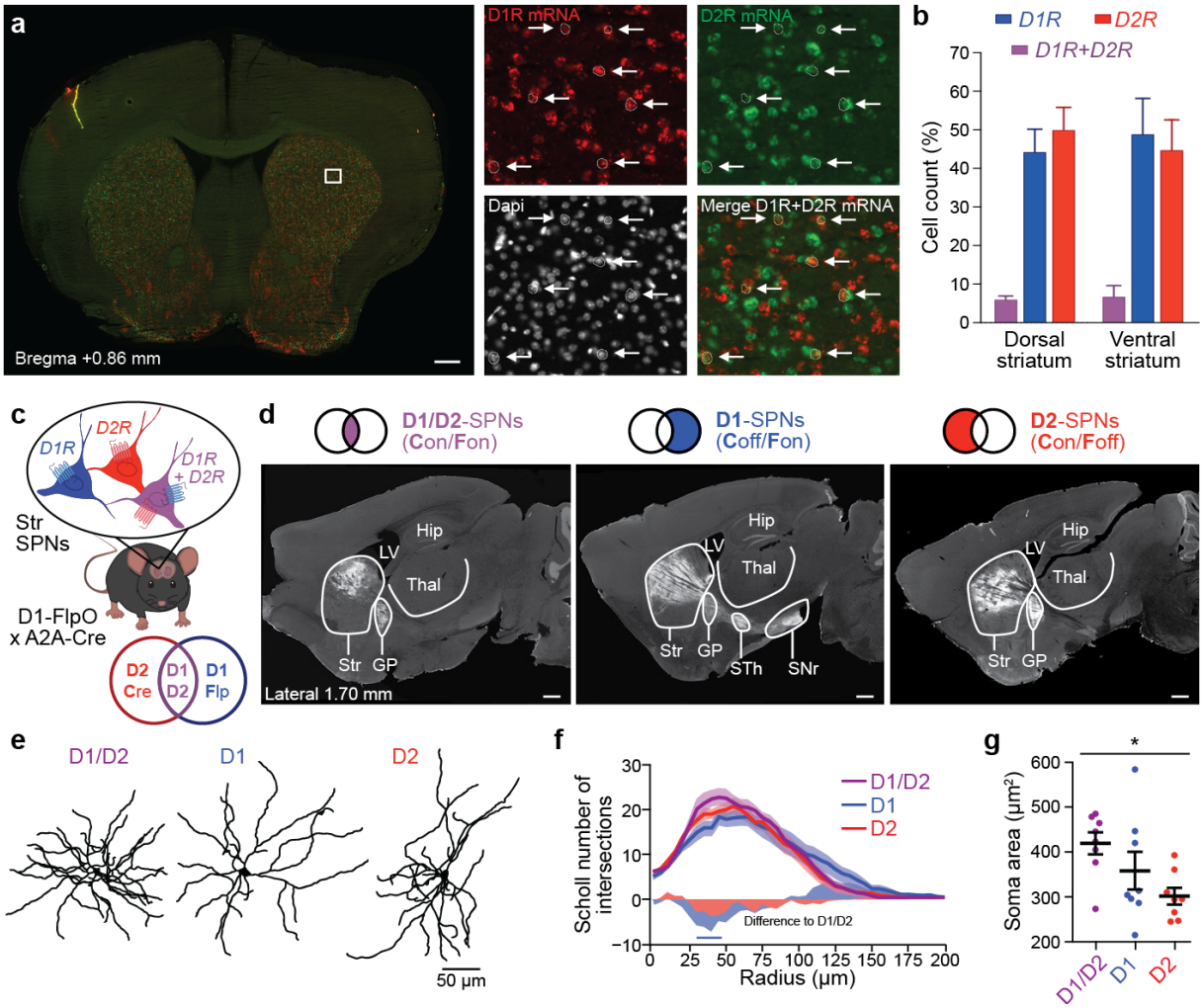

Fig. 1. Morphologically distinct D1/D2 co-expressing SPNs establish an additional efferent striatal pathway. a, Representative coronal section of fluorescent in situ hybridization illustrating D1/D2 co-expression (arrows) in the striatum (scale: left, 1 mm; zooms, 20 µm). **b**, Percentage of D1-, D2-, and D1/D2-positive neurons over cells expressing either D1 or D2 in the dorsal and ventral striatum (n = 3 mice). **c**, Schematic illustrating INTRSECT targeting strategy applied to $D1^{FlpO}/A2a^{Cre}$ mice. **d**, Representative parasagittal sections illustrating projection patterns of D1-, D2-, and D1/D2-SPNs obtained from $D1^{FlpO}/A2a^{Cre}$ mice injected with respective INTRSECT AAV constructs (scale: 500 µm). Abbreviations: Str, striatum; GP, globus pallidus; STh, subthalamic nucleus; SNr, substantia nigra pars reticulate; Thal, thalamus, Hip, hippocampus; LV, lateral ventricle. **(e)** Reconstruction of the dendritic arborisation of representative D1-SPN (left), D2-SPN (middle), and D1/D2-SPN (left). **f-g**, Scholl analysis (**f**) and soma area (**g**) of reconstructed SPNs (D1-SPNs, n = 8; D2-SPNs, n = 8; D1/D2-SPNs, n = 8) (in f, horizontal blue line indicates t-test $p < 0.05$ between D1/D2 and D1; in g, Tukey tests: $*p < 0.05$).

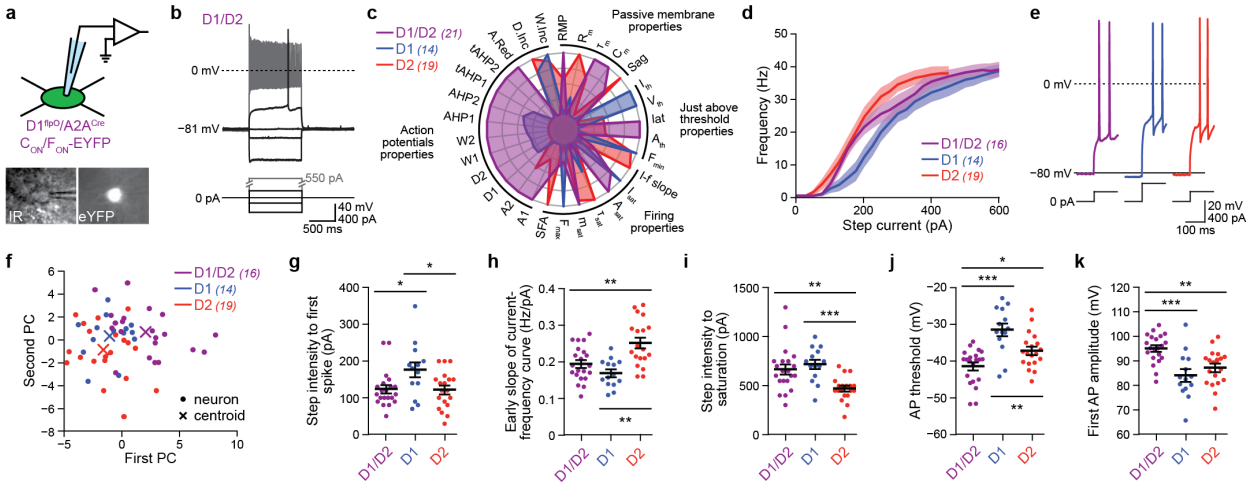

Fig. 2. D1/D2-SPNs differ through unique action potential properties.
a, Diagram of patch-clamp recordings in a YFP labelled D1/D2-SPN (top), and representative photomicrograph under infrared illumination (bottom left) and fluorescent illumination (bottom right). **b**, Typical voltage response of the same D1/D2-SPN in a in response to hyperpolarizing and depolarizing current steps. **c**, Radar plot revealing differences between the three SPN types across all electrophysiological properties extracted. Means for each population are normalized in the range 0-1. **d**, Average current-frequency relationship for the three SPN subpopulations. **e**, Representative examples of action potential (AP) response to depolarizing current in one D1/D2-SPN, one D1-SPN and one D2-SPN. **f**, Two-dimensional projection of the set of neurons recorded (circles) and populations' centroids (cross) following PCA into the first- and second-order components. **g-k**, Quantification of minimal step current to discharge (**g**), early slope of the current-frequency curve (**h**), current intensity to discharge saturation (**i**), AP threshold (**j**), and amplitude of the first AP (**k**) in D1/D2-SPNs (n = 21), D1- (n = 14) and D2- (n = 19) (Tukey's tests: *$p < 0.05$, **$p < 0.01$, ***$p < 0.01$).

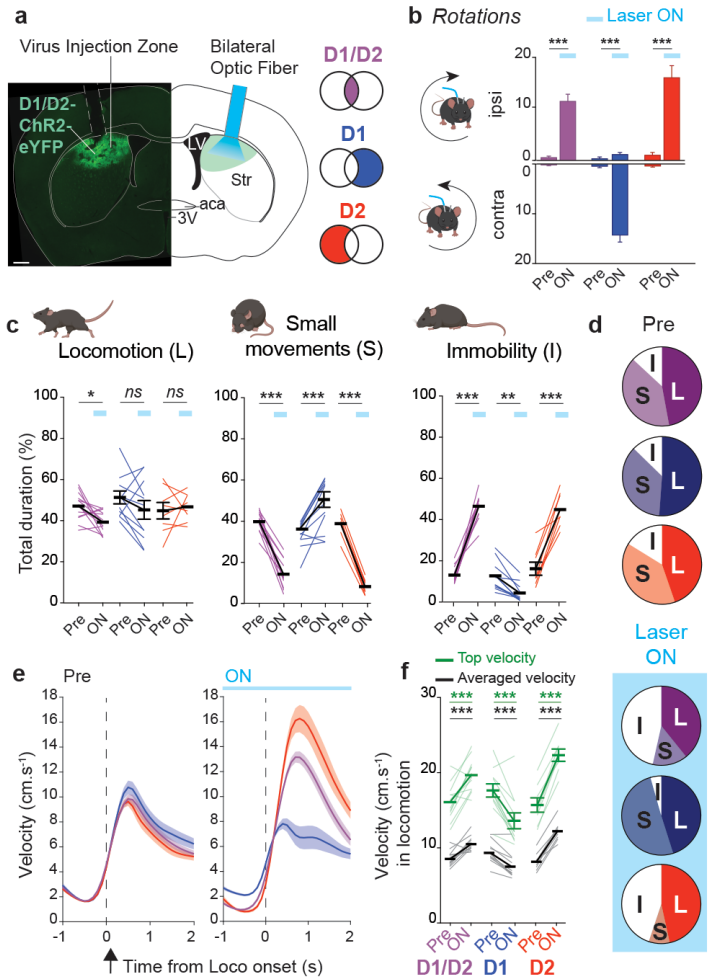

Fig. 3. D1/D2-SPNs activate an indirect pathway that specifically impedes locomotion. **a**, Coronal section and corresponding atlas plane depicting optic fibers placement targeting the dorsal striatum and ChR2 expression in D1/D2-SPNs in $D1^{FlpO}/A2a^{Cre}$ mice (scale: 500µm). **b**, Rotational behaviour elicited by unilateral continuous illumination (60 s) of ChR2-expressing D1/D2-, D1- and D2-SPNs stimulated mice (Tukey's test pre vs. light ON: *** $p < 0.001$). **c**, Effect of bilateral optogenetic stimulation (10 x 30 s trials with 90 s between trials) on time spent in locomotion, small movements, and immobility by free-running mice exploring in open field (Tukey's test pre vs. light ON: * $p < 0.05$; ** $p < 0.01$; *** $p < 0.001$). **d**, Distribution and proportions of the three motor states during baseline (Pre) and stimulation (Laser ON) periods: D1/D2-SPNs Pre: L: 47.1±1.9% | S: 39.8±1.3% | I: 13.1±1.1%; Laser ON: L: 39.2±1.5% | S: 14.3±1.8% | I: 46.5±1.7%; D1-SPNs Pre: L: 51.1±3.1% | S: 36.2±2.0% | I: 12.7±2.1%; Laser ON: L: 45.1±4.5% | S: 50.5±3.8% | I: 4.4±1.4 ; D2-SPNs Pre: L: 44.7±4.0% | S: 39.1±2.0% | I: 16.2±3.2%; Laser ON: L: 46.6±2.4% | S: 8.5±1.3% | I: 44.9±2.9%. **e-f**, Effect of laser stimulation on each group on the averaged temporal evolution of mice velocity around locomotion onset (**e**) and averaged velocity (black) and top velocity (9th decile, green) during locomotion episodes (**f**).

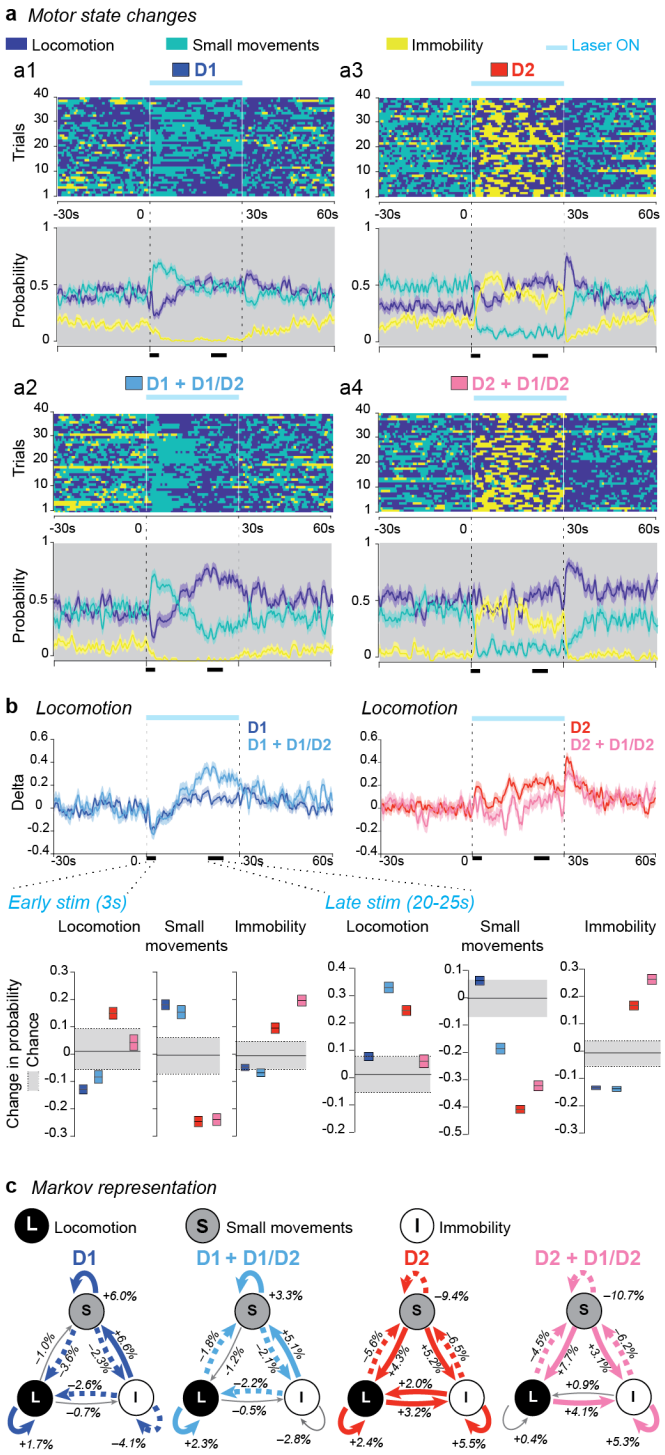

Fig. 4. D1/D2-SPNs orchestrate striatal locomotion by shaping the identity of D1- and D2-SPNs.

a, Motor states for 10 stimulation trials of 4 representative mice of each genotype (top) and corresponding temporal evolution of probability (bottom) to observe locomotion, small movements and immobility, before, during, and after laser stimulation (shading, bootstrap 95% CI). Blue bar, laser stimulation. **b**, Temporal evolution of changes in probabilities to observe locomotion centered on pre-stimulation values (top), and changes in motor state probability induced by laser stimulation during the early (X axis black line, left) and late (X axis black line, right) periods of the photostimulation (colored shading, bootstrap 95% CI for each experimental group; light grey, bootstrap 95% CI for chance). **c**, Changes induced by laser stimulation in conditional transition probabilities between the three motor states for each group evaluated using a Markov chain. Values indicate average change in transition probability and solid and dashed colored lines highlight significant increases and decreases, respectively, during stimulation as compared to baseline period.

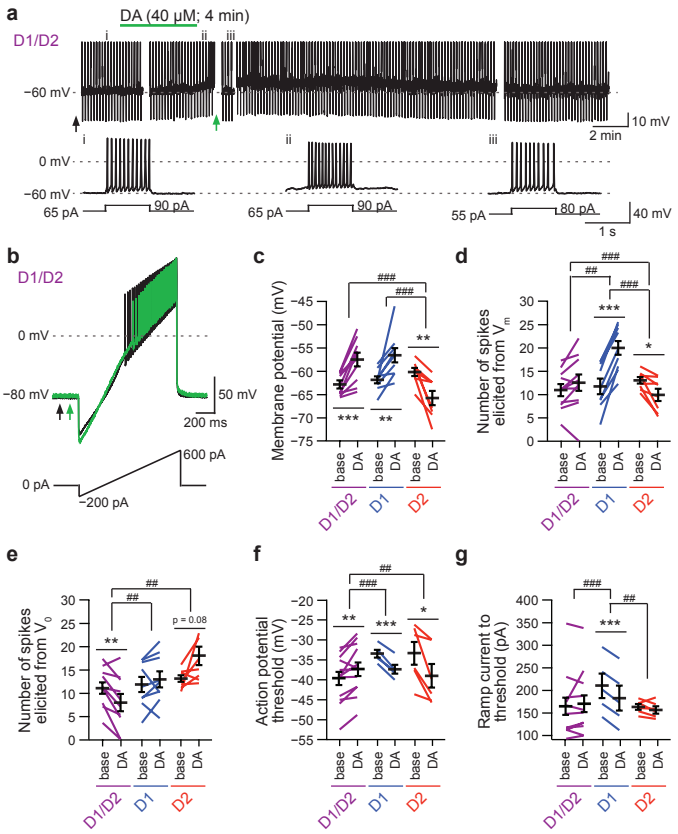

Fig. 5. Co-expression of D1 and D2 cancels dopamine-induced changes in excitability.
a, Effect of bath applied DA (40 µm, 4 min) on membrane potential and evoked firing activity in one D1/D2-SPN (top), and highlight on voltage traces recorded in response to 25 pA depolarizing current steps at times indicated by i-iii (bottom). **b**, Voltage response in one D1/D2-SPN to ramp current injection before (black) and after (green) DA application at times indicated by arrows in **a**. **c-e**, Quantification of DA-induced changes in membrane potential (**c**), number of elicited spiked by a depolarizing pulse from current membrane potential (**d**), and from initial membrane potential (**e**), in D1- (n = 9), D2- (n = 8 [c-d], 7 [e]) and D1/D2-SPNs (n = 11 [c-d], 10 [e]). **f-g**, DA-induced effects on AP threshold (**f**) and minimal ramp current to elicit discharge (**g**) in D1- (n = 5), D2- (n = 6) and D1/D2-SPNs (n = 12) (paired comparison between baseline and after DA application: *p < 0.05, **p < 0.01, ***p < 0.001; magnitude of DA effect between SPN subpopulations: #p < 0.05, ##p < 0.01, ###p < 0.001).

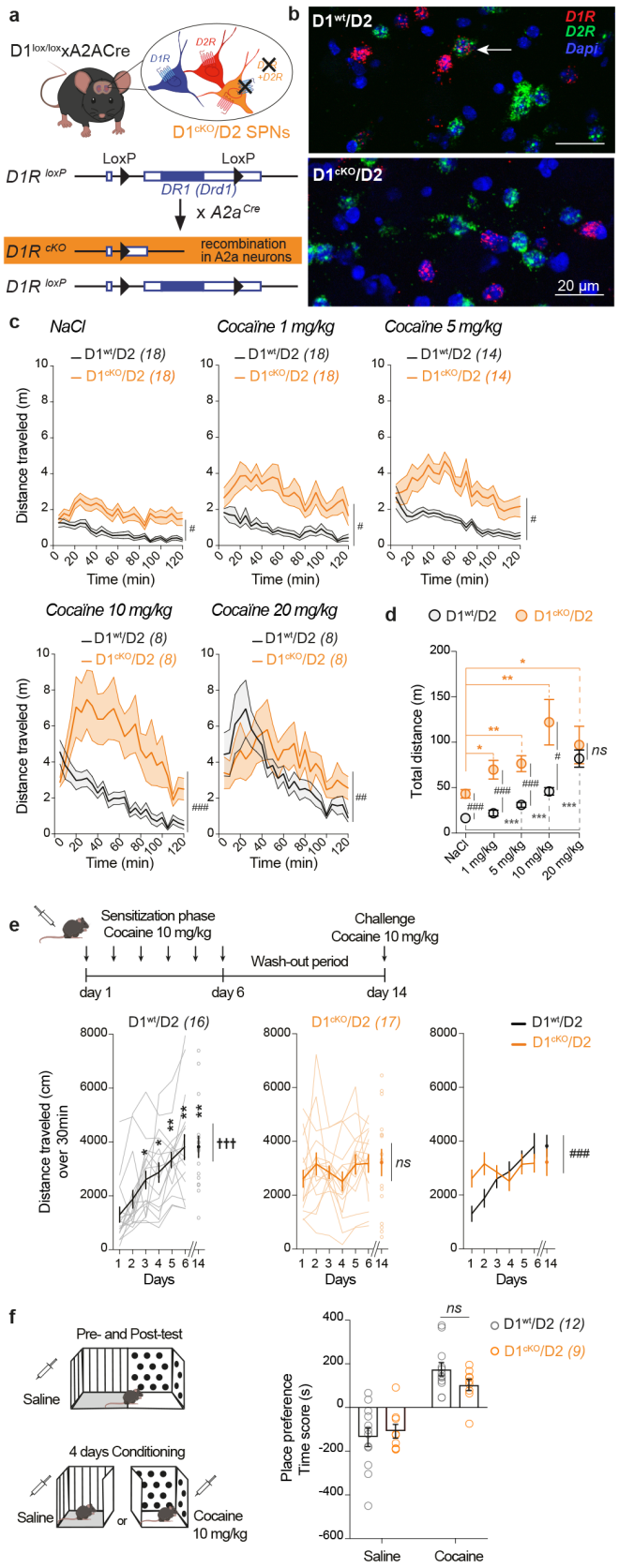

Fig. 6. D1/D2-SPNs are necessary for proper in vivo integration of dopamine signal.

a, Diagram illustrating generation of $D1^{cKO}/D2$ mice.

b, Photomicrographs from RNAscope in $D1^{wt}/D2$ and $D1^{cKO}/D2$ mice illustrating the suppression of DRD1 and DRD2 mRNAs co-expression.

c-d, Temporal distribution of the pro-locomotor effect of acute cocaine injection (**c**) and comparison of the dose-response relationships of the locomotor effect of cocaine in $D1^{wt}/D2$ and $D1^{cKO}/D2$ mice (**d**) (left panels; Sidak's tests $D1^{wt}/D2$ vs. $D1^{cKO}/D2$ for entire duration: $^{\#}p < 0.05$, $^{\#\#}p < 0.01$, $^{\#\#\#}p < 0.001$) (right; Sidak's test $D1^{wt}/D2$ vs $D1^{cKO}/D2$ for each dose: $^{\#}p < 0.05$, $^{\#\#}p < 0.01$, $^{\#\#\#}p < 0.001$, ns not significant; Tukey's tests vs. NaCl : $^{***}p < 0.001$).

e, Effect of repeated 10 mg/kg cocaine injections between $D1^{cKO}/D2$ and $D1^{wt}/D2$ mice on motor activity during 30 min of open field (effect of days for each genotype: $^{\dagger\dagger\dagger}p < 0.001$, ns not significant; post-hoc vs. day1: $^{*}p < 0.05$, $^{**}p < 0.01$; ANOVA interaction days-genotypes: $^{\#\#\#}p < 0.001$).

f, Conditioned place preference for cocaine (10 mg/kg) in $D1^{wt}/D2$ and $D1^{cKO}/D2$ mice (Sidak's tests between genotypes: ns not significant).

Materials and Methods

Generation of transgenic mice

D1-FLPo ($D1^{FlpO}$) mice. $D1^{FlpO}$ mouse strains were engineered at the Mouse Clinical Institute (Institut Clinique de la Souris, MCI/ICS, Illkirch, France). Briefly, the cassette containing the Flipase-O recombinase-T2A-GFP and a floxed NeoR/KanR selection cassette were inserted at the ATG of the D1 dopamine receptor gene by homologous recombination into the RP24-266B BAC (Fig. S2A). The modified BAC after deletion of the selection cassette was microinjected into 300 C57Bl/6N oocytes and several founders have been obtained. F1 offsprings were evaluated for the expression pattern of the Flp-O (Institut Clinique de la Souris, Illkirch, France).

$D1^{loxP/loxP}$ mice. The floxed D1DAR mice were produced as follow. The KOMP ES cell line Drd1tm1a(KOMP)Wts, clone EPD0507_1_B12, derived on the JM8A3.N1 cell line, were obtained from the KOMP Repository at the University of California at Davis (UC Davis). The ES Cells were generated under NIH Grant U01HG004080 by the CHORI-Sanger-Davis (CSD) consortium. Mice were generated from the ES Cells for our research by the UC Davis Mouse Biology Program (MBP), www.mousebiology.org, using blastocyst microinjection, resulting chimeras were mated to C57BL/6NTac mice and heterozygous tm1a (Knockout First) animals were generated through germline transmission. These ES cells are now distributed through the Mutant Mouse Resource and Research Center (MMRRC) at UC Davis, an NIH-funded strain repository, RRID: MMRRC_054799-UCD. For more information on obtaining KOMP products please email mmrrc@ucdavis.edu or go to www.mmrrc.org.

Mice breeding

A2A-Cre ($A2a^{Cre}$) driver line, which expresses the Cre recombinase selectively in D2-SPNs, excluding cholinergic interneurons (*20*) were crossed with $D1^{FlpO}$ mice ($D1^{FlpO}/A2a^{Cre}$) to perform intersectional approaches to target the various SPNs subsets and also used for control conditions. Single transgenic $A2a^{Cre}$ as well as $D1^{FlpO}$ mice were used to assess the functions of classically characterized D2- and D1- "total" SPNs populations, respectively. All mice were of C57BL/6J genetic background.

The brain-specific D1R-depleted mice in A2a expressing neurons ($D1^{cKO}$/D2) were obtained by crossing heterozygote $D1^{loxP/loxP}$ mice with $A2a^{cre}$ mice in order to obtain heterozygous offsprings, which crossed thereby produced wildtype (WT; 7/16), knockout (KO; 3/16) and heterozygote (HET; 6/16) mice at the expected ratio. After weaning and sexing, mice were housed in group of 4-5 animals per cage.

For the collection of *in vivo* optogenetic data only 6-10 weeks old male mice were used. Both females and males were used for *ex vivo* electrophysiology and FISH experiments. Experiments related to $D1^{cKO}$/D2 knockout used both males and females. Two to four mice were housed together, in polycarbonate cages at constant temperature (21±1 °C) and humidity (40–50%), under 12-hour light/dark cycle. Mice were provided with food and water *ad libitum*.

For experiments taking place in place in Belgium, animals were treated according to protocols and guidelines approved by the Institutional Animal Care Committee and were approved by the local ethics committees (ULB Pôle Santé – Protocol 695N). For experiments taking place in France, experimental procedures were approved by the Regional Ethics Committee No. 3 of Ile-de-France region on Animal Experiments and followed the guidelines of the European Communities Council Directive (86/809/EEC) and the Ministère de l'Agriculture et de la Forêt, Service Vétérinaire de la Santé et de la Protection Animale (agreement A 94-028-21). For experiments taking place in Canada, animal housing, breeding, and care were operated in

accordance to the Canadian Council on Animal Care guidelines (CCAC) and all methods were approved by the Animal Care Committee from the Douglas Institute Research Center (protocol number 5570). All methods were performed in accordance with the relevant guidelines and regulations.

Double-probe fluorescent *in situ* hybridization (FISH)

Sample collection. Mice were euthanized by cervical dislocation. Brains were removed, rapidly frozen in cold isopentane (between –30 °C and –35 °C) and have been serially sectioned in 10 series on cryostat at 16 µm thickness. Sections for each brain have been processed by in situ hybridization to allow systematic quantitative analysis throughout the whole dorsal and ventral striatum. Double-probe FISH were performed as previously reported[49].

DNA template for riboprobe synthesis. DNA template with T3 and T7 promoter sequences on both sides of each cDNA target were produced by PCR using promoter-attached primers.

Probes. Double-probe FISH was performed using antisense riboprobes for the detection of the following mRNAs: D1, NM_010076.3 sequence 1756-2707 and D2, NM_010077.3 sequence 268-1187. Synthesis of digoxigenin and fluorescein-labeled RNA probes were made by a transcriptional reaction with incorporation of digoxigenin or fluorescein labelled nucleotides (Sigma-Aldrich; References 11277073910 and 11685619910). Information of primer sequences for riboprobe synthesis is listed in the table below. Specificity of probes was verified using NCBI blast.

PCR primer name	PCR primer sequence	NM	Bases
mDrd1-S-T3	AATTAACCCTCACTAAAGGGATGGAGAAGCTGTCCCCGGCCT	NM_010076.3	1756-2707
mDrd1-AS-T7	TAATACGACTCACTATAGGGGCCTCGGGGAAAGCCTCTGCC		
mDrd2-S-T3	AATTAACCCTCACTAAAGGGAGGAAGCCTCGAGCAGCCGGC	NM_010077.3	268-1187
mDrd2-AS-T7	TAATACGACTCACTATAGGGCTCCTGAGCTCGGCGGGCAG		

Procedure. Cryosections were air-dried, fixed in 4% paraformaldehyde and acetylated in 0.25% acetic anhydride/100 mM triethanolamine (pH 8) followed by washes in PBS. Sections were hybridized for 18 h at 65 °C in 100 µl of formamide-buffer containing 1 µg/ml DIG-labeled riboprobe and 1 µg/ml fluorescein-labeled riboprobe. Sections were washed at 65 °C with SSC buffers of decreasing strength and blocked with 20% FBS and 1% blocking solution. For revelation steps, DIG epitopes were detected with HRP anti-DIG fab fragments at 1:2500 (Sigma-Aldrich; Reference 11207733910) and revealed using Cy3-tyramide at 1:100. Fluorescein epitopes were detected with HRP anti-fluorescein fab fragments at 1:5000 (Sigma-Aldrich; Reference 11426346910) and revealed using Cy2-tyramide at 1:250. Cy2-tyramide and Cy3-tyramide were synthetized as previously described[50]. Nuclear staining was performed with DAPI. All slides were scanned at 20x resolution using the NanoZoomer 2.0-HT (Hamamatsu, Japan). Laser intensity and time of acquisition was set separately for each riboprobe.

Automated quantitative analysis. 10 sections per brain in a total of 3 animals were selected for the quantification. The dorsal and ventral parts of the striatum were differentiated for the quantification. A CellProfiler pipeline[51] was developed to analyze imaging data. Signal segmentation was performed through recognition of objects based on size, shape, intensity, and texture of the signal. All sections were treated with the same segmentation. Cell segmentation was performed on dapi staining to delineate cell surface area. We used the IdentifyPrimaryObject method to identify dapi positive cells with the following parameters: typical diameter of object (15–40 pixels), adaptative threshold strategy, two-classes Otsu thresholding method, and the distinction of clumped objects was based on shape and minimal distance between local maxima of

5 pixels. Next, we established a pixel median threshold value in each fluorescent canal: red (D1-mRNA) and green (D2-mRNA). D1- and D2-positive cells were considered with a median pixel intensity > 0.25 and > 0.10, respectively. We then performed an automated quantitative analysis in which neurons were separated between D1-mRNA only- (dapi + red), D2-mRNA only- (dapi + green) and D1/D2-co-expressing (dapi + red + green) cells in the dorsal and ventral striatum.

RNAScope fluorescent *in situ* hybridization

Frozen brain samples were serially cut using a cryostat (10 µm in thickness) on superfrost-charged slides and kept at −80 °C until further processing. *In situ* hybridization was performed using RNAScope probes and reagents from Advanced Cell Diagnostics and according to the manufacturer's instructions. Briefly, sections were first fixed in chilled 10% neutral buffered formalin for 15 min at 4 °C, dehydrated in increasing gradients of ethanol baths (50%, 70%, 95% 100%, 100%) and left to air dry for 5 min. Endogenous peroxidase activity was quenched with hydrogen peroxide reagent for 10 min, followed by protease digestion for 10 min at room temperature. The following sets of probes were then hybridized for 2 h at 40 °C in a humidity-controlled oven (HybEZ II, ACDbio): MsDrD1 (cat. No. 461901), MsDrD2 (cat. No. 406501-C2) to quantify D1/D2 coexpression. Successive addition of amplifiers was performed using the proprietary AMP reagents, and the signal visualized through probe-specific horseradish-peroxidase-based detection by tyramide signal amplification with Opal dyes (Opal 520 and Opal 570; Perkin Elmer) diluted 1:300. Slides were then coverslipped with Fluoromount-G mounting medium with 4,6-diamidino-2-phenylindole (DAPI) for nuclear staining (Invitrogen Fisher, cat. No. 501128966) and kept at 4 °C until imaging.

Virus-mediated targeting of channelrhodopsin and eYFP expression

We used an intersectional optogenetic viral strategy to trace, record from and control each SPNs population, involving the stereotaxic injection of $D1^{FlpO}/A2a^{Cre}$ mice with INTRSECT viruses[33] transfecting cells with eYFP-tagged ChR2(H134R), or eYFP alone for *ex vivo* recordings and control mice, in a manner conditional on the presence of Cre (**C**) and/or FlpO (**F**) in three configurations: **C**off/**F**on, **C**on/**F**off and **C**on/**F**on, targeting respectively D1-, D2- and D1/D2-SPNs (AAV(DJ)-nEF-**C**on**F**on / **C**off**F**on / **C**on**F**off-hChR2(H134R)-eYFP, AAV(DJ)-hSyn-**C**on**F**on / **C**off**F**on / **C**on**F**off-eYFP; some aliquots were kindly provided by Charu Ramakrishnan and Karl Deisseroth at Stanford University, and most viral vectors were packaged and provided by UNC vector core, North Carolina). To compare ChR2-induced effects in response to photostimulations in these three exclusive SPNs populations with those classically described in mixed direct D1-expressing SPNs (combining D1- and D1/D2-SPNs) and mixed indirect D2-expressing SPNs (combining D2- and D1/D2-SPNs), we also expressed ChR2 in $D1^{FlpO}$ and $A2A^{Cre}$ mice using FRT-ChR2 and lox-ChR2 constructs, respectively (AAV(DJ)-EF1a-fDIO-hChR2(H134R)-eYFP, AAV(5)-EF1a-DIO-hChR2(H134R)-eYFP; UNC vector core).

At 8–10 weeks old, mice used for tracing and *in vivo* experiments, or at about 6 weeks old, mice used for *ex vivo* experiments were anesthetized with isoflurane (4% induction, 1% maintenance; 0.5 L/min O2). 2x1 µL of recombinant AAV listed above were bilaterally injected under stereotaxic control into the dorsal striatum (anteroposterior (AP), +0.8 mm; mediolateral (ML), 1.5 mm; dorsoventral (DV), –2.7 mm, relative to Bregma) through a 30 G cannula at a rate of 100 nL/min. The injection needle was lowered through a hole drilled lateral to the midline (AP, +0.8 mm; ML, 1.5 mm). Mice were allowed to recover for 10 days before being habituated to patchcord connections and experiments started at least 3 weeks after viral injections.

Ex vivo electrophysiology experiment recording and analysis

Experiment preparation. In preparation for electrophysiology, brain slices containing the dorsal striatum were obtained from mice injected as described above. Under deep anesthesia the animals were decapitated and brains were quickly removed. Coronal slices (250 µm thick) were cut with a vibrating microtome (VT1000S; Leica) in ice-cold (4 °C) slicing artificial cerebrospinal fluid (ACSF) containing the following (in mM): 140 choline chloride, 2.5 KCl, 1.25 NaH_2PO_4, 7 $MgCl_2$, 0.5 $CaCl_2$, 25 $NaHCO_3$, 14 D-glucose, pH 7.3, and constantly oxygenated (95% O2/5% CO2). Slices were transferred to the incubation chamber filled with ACSF containing (in mM): 124 NaCl, 2.5 KCl, 1.2 NaH_2PO_4, 2 $CaCl_2$, 1 $MgCl_2$, 26 $NaHCO_3$, 10 D-glucose. Slices were incubated for 1 h at 34 °C and then maintained at room temperature.

Whole cell recordings. Slices were placed on the stage of an Axio Examiner.A1 microscope (Carl Zeiss), equipped with an infrared CCD camera (ORCA-05G; Hamamatsu), and visualized by under infrared (IR) illumination. Slices were maintained immersed and continuously surperfused at 2–5 mL/min with oxygenated ACSF. Neurons in the dorsal striatum were selected based on eYFP expression using 470 nm LED light (OptoLED, Carin Research) visualized through FITC/Cy2 filter set (Carin Research). All electrophysiological experiments were performed with an EPC-10 patch-clamp amplifier (HEKA) attached to a computer running PatchMaster software (HEKA). Signals were low-pass filtered at 2.9 kHz and digitalized at 20 kHz. Whole-cell patch-clamp recordings were performed with patch micropipettes (6–8 MΩ) pulled from borosilicate glass capillary tubes (1.5 mm outer diameter, 0.225 mm wall thickness; Hilgenberg) on a vertical puller (PIP5; HEKA) filled with 8 µl of internal solution containing the following (in mM): 105 K-gluconate, 30 KCl, 10 4-(2-hydroxyethyl)-1-piperazineethanesulfonic acid, 0.3 ethylene glycol-bis(β-aminoethyl ether)-N,N,N',N'-tetraacetic acid, 10 Na_2-phosphocreatine, 4 Mg_2-ATP, 0.3 Na_2-GTP, pH 7.4, 290–300 mOsm, and 3 mg/mL biocytin. For *ex vivo* optogenetic stimulation, pulses of blue light (470 nm) were delivered using LEDs (OptoLED, Cairn Research) controlled by PatchMaster (HEKA) through the EPC-10 patch-clamp amplifier (HEKA).

Recording analysis. The intrinsic membrane properties of neurons were assessed by applying current steps (1 s) from –500 pA to firing saturation in 10 pA increments. To comprehensively describe the electrophysiological properties of recorded SPNs, 30 parameters reflecting the properties of SPNs[35-37, 52] measured on traces corresponding to the voltage responses induced by hyperpolarizing and depolarizing current pulses. These parameters are following the Petilla nomenclature[53]. (1) Resting membrane potential (RMP) was measured immediately after electrical access to the intracellular compartment of the cell. (2) Input membrane resistance (R_m), (3) membrane time constant (τ_m), and (4) membrane capacitance (C_m) were determined in response to hyperpolarizing current pulses resulting in voltage drops of 10–15 mV relative to rest. R_m was measured following Ohms law and τ_m was computed as the time constant of a single exponential fit of the voltage response from onset to maximum hyperpolarization. C_m was obtained following the formula $C_m = \tau_m/R_m$. Some neurons have been described to undergo a partial repolarization following a hyperpolarization peak in response to negative currents. To quantify this, whole-cell conductance was measured when the sag conductance was inactive (G_{hyp}) or active (G_{sag}). G_{sag} was measured as the slope of the linear portion of a current–voltage (I–V) plot, in which V was determined at the end of 1 s hyperpolarizing current pulses (–500 to 0 pA) and G_{hyp} as the slope of the linear portion of the I–V plot where V was determined as the maximal negative potential during the 1 s hyperpolarizing pulses. (5) Sag index was calculated as a relative decrease in membrane following $(G_{sag} - G_{hyp})/G_{sag}$. (6) Step intensity to first spike (I_{th}) was evaluated as the minimal intensity of the 1 s current pulse that elicited an action potential. As SPNs display a delayed firing supported by I_A currents, (7) first spike latency (lat) was computed as the time needed to elicit a

spike after the onset of a current pulse corresponding to the step intensity to first spike. (8) Action potential threshold (V_{th}) was measured as the potential of first spike onset when the rate of membrane potential change exceeded 30 mV/ms. To describe the firing behaviour of recorded SPNs around threshold, the instantaneous firing frequency measured in response to the minimal current injection eliciting more than 3 action potentials was and fitted to a linear curve with (9) adaptation (A_{th}) corresponding to the slope of the linear fit and (10) minimal steady state frequency (F_{min}) corresponding to its y-intercept ($F(t) = A_{th} \times t + F_{min}$). Then to evaluate the change in firing activity in relation with increased depolarizing current steps (11) the slope of the current-frequency relationship (I–f slope) was calculated in its initial linear portion. (12) The step intensity to saturation (I_{sat}) was defined as the maximal 1 s current pulse eliciting robust firing activity without inducing firing saturation. At high firing frequencies, neurons display spike frequency adaptation which is characterized by an early exponential decrease in spike frequency followed by a linear decrease. To quantify this adaptation, the instantaneous firing frequency during the train of spike induced by the maximal depolarizing current injected not inducing saturation was fitted to decaying single exponential and of a linear function using the following formula $F(t) = A_{sat} \times \exp(-t/\tau_{sat}t) + m_{sat} \times t + F_{max}$[54] using the fitting parameters defined as (13) amplitude of early adaptation (A_{sat}), (14) time constant of early adaptation (τ_{sat}), (15) slope of late adaptation (m_{sat}), and (16) maximal steady state frequency (F_{max}). To evaluate firing adaptation at an intermediate level of activation (17) spike frequency adaptation (SFA) was measured as the ration between the instantaneous firing frequency between the first two spikes over the instantaneous firing frequency over the last three spikes on traces corresponding to the depolarizing current injection eliciting a sustained action potential train of about 20 spikes. Spike waveforms have been described to vary between neuronal cell types. To quantify these variations, 6 parameters were measured on the first and second spikes of traces corresponding to the depolarizing current injection eliciting a sustained action potential train of about 20 spikes. (18,19) The amplitudes of the first (A1) and second action potential (A2) were defined as the difference of membrane potential between their onsets and peaks. (20,21) Spike durations of the first (D1) and second spike (D2) were defined the spike with between spike onset and spike offset. (22,23) Spike half-widths of the first (W1) and second spike (W2) were defined as the spike width at half amplitude. (24,25) After hyperpolarization potential (AHP) maximums (AHP1 and AHP2) were calculated using the membrane potential at the onset of the action potential as a reference. Comparatively, (26,27) AHP latencies (tAHP2 and tAHP2) were calculated as the time span between the AHP maximum and the onset of the action potential. During a spike train, spikes can display variations in their amplitude and duration. In order to quantify this phenomenon, (28) amplitude reduction (A.Red), (29) duration increase (D.Inc), and (30) half-width duration increase (W.Inc) were computed as (A1 – A2)/A1, (D2 – D1)/D1, and (W2 – W1)/W1, respectively.

Pharmacology. The following drugs were used: dopamine HCl (40 µM, Sigma-Aldrich); sulpiride (10 µM, Sigma-Aldrich); and SCH23390 (10 µM, Sigma-Aldrich). Stock solutions of these compounds were stored as frozen aliquots at –20 °C and dissolved in ACSF to their working concentrations immediately before application. Pharmacological experiments were carried out in current-clamp mode. Neurons were depolarized to about –60 mV by injecting holding current. Changes in membrane voltage were measured at this holding current. To elicit firing activity and quantify membrane resistance, neurons were stimulated using a 1 s depolarizing pulse set to elicit 10–15 action potentials and after 1 s held at holding current neurons were stimulated with a –50 pA hyperpolarizing pulse from holding current lasting 500 ms. This stimulation protocol was repeated every 10 s throughout the recording. Moreover, a current ramp (1 s from –200 pA to 600 pA) was applied during baseline and at the peak of pharmacological effect to extract action potential

threshold and current to first action potential as well as interpolate current-frequency curves. Recordings were discarded if access resistance changed by more than 20% throughout the experiment. Results are not corrected for liquid junction potential.

Three-dimensional reconstruction of biocytin-filled SPNs

Brain slices containing SPNs filled with biocytin, were incubated overnight at 4 °C in paraformaldehyde solution (4% PFA in 0.01 mM PBS). Slices were then washed in PBS and permeabilized in PBS with 0.1% TritonX-100 (Sigma-Aldrich). Slices were incubated with streptavidin-coupled AlexaFluor488 (1:200, Jackson ImmunoResearch) for 2 h at room temperature under constant agitation. After wash in PBS, slices were mounted with Fluorsave medium (Fisher Scientific) between slide and coverslip (VWR).

Serial optical sections in the X, Y and Z planes (Z-stacks) were acquired on a laser-scanning confocal system (LSM 510; Zeiss) mounted on an Axiovert 200M inverted microscope (Zeiss) and equipped with a LD c-Apochromat 40×/1.2W objective (Zeiss). The excitation beam of an argon laser (488 nm) was used and the fluorescence was measured between 500 and 550 nm for the detection of the Alexa 488 fluorophore. Once acquired, ZEN software (Zeiss) was used to stitch the images. Manual reconstruction of the dendritic arborization of the neurons was done with the help of the computer filament tracing function in the 3D image analysis software Imaris (Bitplane, Ireland). Total dendritic arborization reconstruction allowed the study of dendrite branching and length, and sholl analysis. The soma volume was automatically measured by creating a surface that delineated the soma region.

Optic fiber implantation for *in vivo* experiments

At 8–10 weeks old, within the same surgery following virus injection, mice subjected to in vivo experiments were implanted with homemade bilateral optic fiber implants. A cleaved piece of optic fiber ~12 mm in length (400 µm diameter, NA 0.39; Thorlabs) was inserted and glued into a metal ferrule (1.25 mm diameter; Thorlabs). Optic fiber implants that were inserted were verified before implantation to display at least 80% of light transmission with laser power set to reach 6–8 mW at the tip of both fibers. During the surgery, before viral injection, the skull was completely cleared of all connective tissue and thoroughly dried using alcohol. To insert the optic fiber implant, a hole was drilled in the skull at the following coordinates: AP, +0.9 mm; ML, 2.17 mm, relative to Bregma. After gently cutting through the dura, the implant was lowered through the hole at an angle of 10° with the optic fiber end location targeted 400 µm above the injection site in the dorsal striatum. Following optic fiber placement, dental cement (Metabond) was applied to secure the implant permanently to the skull.

Rotational behavior

Animals were placed in circular chambers (17 cm diameter) to examine rotational behavior under unilateral stimulations. A camera (Basler ace acA1600-60gc) was placed above the chambers to record videos at 30 frames/sec, and rotations were scored manually. Rotations were defined as each 360° rotation that contained no turn of more than 90° in the opposite direction. We analyzed them over three periods 'Pre' period, which corresponded to 60 s preceding laser illumination; 'ON' period, which corresponded to constant 60 s unilateral laser illumination (473 nm, Laserglow); and 'OFF' period of 60 s at the end of laser illumination. Both right and left hemisphere laser illuminations were performed in a randomized manner in two distinct trials separated by a 1-2 h interval period during which mice returned in their home cage.

Open-field paradigm

Open field (OF) is a white square enclosure of 40 x 40 cm where animals can move freely and are video-monitored from above (Basler ace acA1600-60gc; sampling rate 30 frames/sec). Detection and calculation of animal's center of mass coordinates were performed using Ethovision xt 14.0 software (Noldus). Animal's speed was calculated from changes in center of mass coordinates between two successive frames and smoothed (moving average, 0.5 s width) to reduce noise and tracking artifacts. Animal's behavior in the OF was then classified into three motor states: locomotion when speed exceeds 2 cm/s and stays above 2 cm/s for at least 0.5 s; immobility when speed stays below 0.5 cm/s for at least 0.5 s; and small movement when speed lays between 0.5 cm/s and 2 cm/s. Any unassigned bout (lasting shorter than 0.5 s) is affected for its first half to the previous state and for its second halt to the next state.

Animals were recorded for a 10 min reference baseline period before any laser illumination ('Pre' period). Mice exhibiting a biased low baseline activity measured as distance traveled below 1700 cm over the 10 min baseline were excluded from analysis. Then the laser was illuminated in a series of ten trials. Each trial lasted 30 s with constant illumination ('ON' period), followed by a 90 s period during which the laser was turned off ('OFF' period). The total time spent in each motor state, the frequency and the mean episode duration of each state were calculated over the 10 min baseline ('Pre'), and over the average of the 10 trials for the 'ON' and 'OFF' periods.

To better characterize how each SPN population activation affects motor states dynamics we computed transition probabilities between states using a Markov chain model from time series of motor states resampled at 5 Hz. Briefly, for each time period ('Pre', 'ON', 'OFF') defined above and for each mouse we calculated the transition probability from state X to Y P(Y|X) as the number of time bins in state X immediately followed by state Y over the total number of time bins in state X.

To catch supplementary information on the dynamics of motor states during laser illumination, we also computed probabilities to observe motor states for all stimulation trials. The 95% CI for motor state probability were calculated using bootstrap from time series of motor states resampled at 10 Hz. For each experimental group, we repeatedly resampled data aligned to laser illumination (from 30 s before laser onset to 30 s after laser offset) by randomly generating the same number of total trials (random sampling with replacement). For each of the 10,000 random iterations, we calculated the mean probability to observe each motor state across trials. The lower and upper CIs were obtained for each time point from the distribution of resampled mean values. The 95% CI for changes in probabilities were obtained the same way by calculating the difference in mean probabilities during early (from 0 s to 3 s after laser onset), intermediate (from 5 s to 10 s after laser onset), and late (from 20 s to 25 s after laser onset) periods of laser illumination minus mean probabilities before laser illumination (over 10 s before laser onset). Chance levels for changes in probabilities were calculated the same way by selecting a random time point for trial onset. 95% CIs for actual trials lying outside the 95% CI for chance are considered significantly different.

For OF experiments performed on $D1^{cKO}$/D2 mice and their wildtype littermates, mice were placed in the OF and video-tracked for 60 min.

All these analyses were performed using Matlab (Mathworks).

Histological confirmation of optic fiber placement and construct expression

Following completion of all behavioral optogenetic experiments, mice were deeply anesthetized with one injection of avertin (2,2,2-tribromoethanol 1.25%, 2-methyl-2-butanol 0.78%; 20 µl/g, intraperitoneal, Sigma-Aldrich). Mice were then perfused transcardially with 1X

PBS, pH 7.4, followed by 4% paraformaldehyde in PBS (PFA). The brains were then extracted and postfixed overnight in PFA at 4 ºC and subsequently cryoprotected in 30% sucrose dissolved in PBS for an additional 24 h at 4 ºC. Each brain was then frozen and sectioned at 40 µm using a cryostat. To confirm construct expression and optic fiber placement, 1:3 sections over the entire striatum were first washed in PBS 1X-Triton (0.3 %) (PBST), incubated in blocking solution (10% donkey serum (DS) in PBST) for 1 h at room temperature and subsequently incubated for 1 h with GFP boosters (ATTO488, Chromotek) diluted 1:400 in 1% DS. Sections were then counterstained for 10 min with the chromosomal dye Hoechst 33258 (prepared in 1X PBS at 1:10,000) and then mounted on glass slides and permanently coverslipped with Fluoromount. Fluorescent images were collected using a fluorescent microscope (V16, Zeiss). Only mice with histologically confirmed bilateral correct placement of optic fiber as well as proper construct expression in the dorsal striatum were used in the present study.

Psychostimulant dose-response and behavioral sensitization

Locomotor response to acute psychostimulant treatment was assessed by intraperitoneal administration of a single dose of amphetamine HCl (0, 1, 3 mg/kg in 0.9% saline) or cocaine HCl (0, 1, 5, 10, 20 mg/kg in 0.9% saline) to $D1^{cKO}$/D2 mice and their wild-type littermates. The test environment consists in transparent activity boxes (VersaMax automated activity monitor, AccuScan Instruments Inc., Columbus, OH) measuring 42 cm x 42 cm x 30 cm. Mice were first habituated to the environment by being placed in the activity boxes for 20 min daily for 3 consecutive days. Acute injections were made on day 4: mice were individually placed in activity boxes for 15 min, and after injection were immediately placed back in the boxes for an additional 120 min period. Locomotor activity was recorded in 5 min intervals.

In order to induce behavioral sensitization, $D1^{cKO}$/D2 mice and their wild-type littermates received daily administration of cocaine (10 mg/kg) for 6 consecutive days. On day 14, a challenge dose of cocaine (10 mg/kg) was administered to both groups. Injections were made 15 min after placing the mice in the monitor boxes and locomotion recording continued for 120 min after cocaine administration.

Conditioned Place Preference

The Pavlovian conditioning protocol, using distinctive floor textures as conditioned stimuli, was adapted from Cunningham et al., (1999)[55] . The apparatus consisted of a Plexiglas box divided into two compartments (5 cm wide, 15 cm long, 15 cm high), with interchangeable floors made of either stainless steel or plastic. Each apparatus was equipped with photocell beams allowing automatic recording of the animal's position and horizontal activity. The experiment involved three phases during which each animal was weighed and injected immediately before being placed in the apparatus. (i) During the habituation session, each animal received saline and had free access to both compartments with distinctive floors for 30 min. (ii) The conditioning phase (eight sessions) lasted four consecutive days, with two 30 min trials a day. Mice were restricted to a single compartment, with the less preferred floor paired four times with cocaine (10 mg/kg, 10 mL/kg, intraperitoneal) and the other floor texture paired four times with saline. (iii) Place preference was assessed 24 h after the last conditioning trial. All animals received a saline injection before being exposed to both compartments with distinctive floors for 30 min. The cocaine-conditioned preference was determined by comparing the time spent in the cocaine associated box post versus pre-chronic injection.

Statistics Analysis

Statistical analysis was performed using GraphPad Prism 7.0e and Matlab. All data are presented as mean ± standard error of the mean (SEM) except explicitly stated otherwise. Statistical significance was set at 0.05 for all procedures. Normality and homoscedasticity assumptions were verified prior to the use of any parametric tests (Shapiro-Wilk normality test and equality of variances *F-test*). In case of violation of any of these assumptions, standard transforms were applied to meet the above criteria. Statistics were performed with repeated measures two-ways or three-ways ANOVAs to test the significance between experimental groups (genotype) and stimulation conditions (in case of optogenetics), or groups (floxed and wild-type litermates), drugs and time. Statistic tests details are available in the statistical table below. Cell count and in vivo analyses were performed by researchers blinded to genotype and experimental condition.

Detailed statistical analysis for Figures, extended Figures and extended Table:

Figure number	n	Statistical method	F/t value	p value	Post hoc multiple comparisons
Figure 1f	D1/D2: 8 cells D1: 8 cells D2: 8 cells	2-way ANOVA with one factor replication	Geno F(2,21)=0.14 Radius F(203,4263)=143.6 Geno x radius F(206,4263)=1.79	Geno P=0.8691 Radius P<0.0001 Geno x radius P<0.0001	Comparisons between each pairs of genotypes for all radius bins D1 vs D2: P>0.05 all bins D1 vs D1/D2: P<0.05 between 31µm and 51µm D2 vs D1/D2: P>0.05
Figure 1g	D1/D2: 8 cells D1: 8 cells D2: 8 cells	One way ANOVA	F(2,21)=3.86	P=0.0374	D1 vs D2: P=0.3858 D1 vs D1/D2: P=0.3443 D2 vs D1/D2: P=0.0292
Extended Data Figure 1b	10 sections per mouse 3 mice	Friedman test	$X^2(10)= 11.29$	P=0.256	
Figure 2g-k Extended Data Table 1	D1/D2: 21 cells D1: 14 cells D2: 19 cells	One-way ANOVA	F(2,51) See Extended Data Table 1	See Extended Data Table 1	See Extended Data Table 1
Figure 3b	Shown: D1/D2: 13 mice D1: 12 mice D2: 9 mice Not shown: D1 + D1/D2: 9 mice D2 + D1/D2: 6 mice D1/D2^{ctl}: 7 mice	2-way ANOVA with one factor replication	Stim x Genotype F(10,100)=9.957 Stim F(2,100)=204.4 Genotype F(5,50)=7.855	Stim x Genotype P<0.0001 Stim P<0.0001 Genotype P<0.0001	Pre vs Stim | Pre vs Post | Stim vs Post: D1/D2: P<0.0001 | P=0.937 | P<0.0001 D1: P<0.0001 | P=0.903 | P<0.0001 D2: P<0.0001 | P=0.785 | P<0.0001 D1 + D1/D2: P<0.0001 | P=0.985 | P<0.0001 D2 + D1/D2: P<0.0001 | P=0.135 | P<0.0001 D1/D2^{ctl}: P=0.981 | P=0.981 | P>0.999
Figure 3c Extended Data Figure 4a (left) Locomotion	D1/D2: 13 mice D1: 11 mice D2: 8 mice D1+D1/D2: 6 mice D2+D1/D2: 5 mice D1/D2^{ctl}: 7 mice	2-way ANOVA with one factor replication	Stim x Genotype F(10,88)=1.973 Stim F(2,88)=4.321 Genotype F(5,44)=2.511	Stim x Genotype P=0.0458 Stim P=0.00162 Genotype P=0.0439	Pre vs LaserON | Pre vs LaserOFF | LaserON vs LaserOFF : D1/D2: P=0.0309 | P=0.0061 | P=0.8301 D1: P=0.1647 | 0.0756 | P=0.9263 D2: P=0.8837 | 0.0416 | P=0.0118 D1+D1/D2: P=0.3408 | P=0.8715 | P=0.1422 D2+D1/D2: P=0.9863 | P=0.4414 | P=0.3538 D1/D2^{ctl}: P=0.9974 | P=0.4466 | P=0.4870
Figure 3c Extended Data Figure 4b (left) Small movements	D1/D2: 13 mice D1: 11 mice D2: 8 mice D1+D1/D2: 6 mice D2+D1/D2: 5 mice D1/D2^{ctl}: 7 mice	2-way ANOVA with one factor replication	Stim x Genotype F(10,88)=35.49 Stim F(2,88)=60.18 Genotype F(5,44)=7.584	Stim x Genotype P<0.0001 Stim P<0.0001 Genotype P<0.0001	Pre vs LaserON | Pre vs LaserOFF | LaserON vs LaserOFF : D1/D2: P<0.0001 | P=0.5739 | P<0.0001 D1: P<0.0001 | P=0.9527 | P<0.0001 D2: P<0.0001 | P=0.9940 | P<0.0001 D1+D1/D2: P=0.7258 | P=0.6762 | P=0.2471 D2+D1/D2: P<0.0001 | P=0.4673 | P<0.0001 D1/D2^{ctl}: P=0.5109 | P=0.9031 | P=0.7763
Figure 3c Extended Data Figure 4c (left) Immobility	D1/D2: 13 mice D1: 11 mice D2: 8 mice D1+D1/D2: 6 mice D2+D1/D2: 5 mice D1/D2^{ctl}: 7 mice	2-way ANOVA with one factor replication	Stim x Genotype F(10,88)=27.86 Stim F(2,88)=44.02 Genotype F(5,44)=10.55	Stim x Genotype P<0.0001 Stim P<0.0001 Genotype P<0.0001	Pre vs LaserON | Pre vs LaserOFF | LaserON vs LaserOFF : D1/D2: P<0.0001 | P=0.0124 | P<0.0001 D1: P=0.0098 | P=0.0133 | P<0.0001 D2: P<0.0001 | P=0.0089 | P<0.0001 D1+D1/D2: P=0.0558 | P=0.3864 | P=0.0012 D2+D1/D2: P<0.0001 | P=0.8938 | P<0.0001 D1/D2^{ctl}: P=0.5569 | P=0.1672 | P=0.7098
Figure 3e Extended Data Figure 4d	D1/D2: 13 mice D1: 11 mice D2: 8 mice D1+D1/D2: 6 mice D2+D1/D2: 5 mice D1/D2^{ctl}: 7 mice	3-way ANOVA with two factors (time, stim) replication	Genotype F(5,44)=1.79 Time F(60,2640)=714.03 Geno x time F(300,2640)=5.84 Stim F(2,88)=12.50 Geno x stim F(10,88)=10.31 Time x stim F(120,5280)=20.55	Genotype P=0.135 Time P=2.1e-88 Geno x time P=3.9e-10 Stim P=0.000158 Geno x stim P=1.1e-8 Time x stim P=3.6e-34 Geno x time x stim P=2.4e-37	Difference with D1/D2 Time points: 1.1s/1.2s/1.3s D1: p<0.0001/ p<0.0001 / p=0.0017 D2: p=0.052 / p=0.053 / p=0.0480 D1 + D1/D2: p<0.0001/ p=0.0017 / p=0.0047 D2 + D1/D2: p=0.350/ p=0.462 / p=0.592 D1/D2^{ctl}: p<0.0001/ p=0.0110 / p=0.027

			Geno x time x stim F(600,5280)=6.90		
Figure 3f Extended Data Figure 4e Averaged velocity (black)	D1/D2: 13 mice D1: 11 mice D2: 8 mice D1+D1/D2: 6 mice D2+D1/D2: 5 mice D1/D2^{ctl}: 7 mice	2-way ANOVA with one factor replication	Stim x Genotype F(10,88)=33.62 Stim F(2,88)=46.96 Genotype F(5,44)=3.228	Stim x Genotype P<0.0001 Stim P<0.0001 Genotype P=0.0144	Pre vs LaserON | Pre vs LaserOFF | LaserON vs LaserOFF : D1/D2: P<0.0001 | P=0.0431 | P<0.0001 D1: P<0.0001 | P=0.0182 | P=0.0010 D2: P<0.0001 | P=0.3269 | P<0.0001 D1+D1/D2: P=0.0020 | P=0.4876 | P=0.0518 D2+D1/D2: P<0.0001 | P=0.5952 | P<0.0001 D1/D2^{ctl}: P=0.8971 | P=0.1641 | P=0.3498
Figure 3f Extended Data Figure 4e Top velocity (green)	D1/D2: 13 mice D1: 11 mice D2: 8 mice D1+D1/D2: 6 mice D2+D1/D2: 5 mice D1/D2^{ctl}: 7 mice	2-way ANOVA with one factor replication	Stim x Genotype F(10,88)=25.02 Stim F(2,88)=22.09 Genotype F(5,44)=3.601	Stim x Genotype P<0.0001 Stim P<0.0001 Genotype P=0.0081	Pre vs LaserON | Pre vs LaserOFF | LaserON vs LaserOFF : D1/D2: P<0.0001 | P=0.0309 | P<0.0001 D1: P<0.0001 | P=0.0090 | P=0.0021 D2: P<0.0001 | P=0.3199 | P<0.0001 D1+D1/D2: P=0.0001 | P=0.2858 | P=0.0163 D2+D1/D2: P<0.0001 | P=0.4170 | P=0.0016 D1/D2^{ctl}: P=0.3042 | P=0.0485 | P=0.6328
Extended Data Figure 4a (middle) Bout number Locomotion	D1/D2: 13 mice D1: 11 mice D2: 8 mice D1+D1/D2: 6 mice D2+D1/D2: 5 mice D1/D2^{ctl}: 7 mice	2-way ANOVA with one factor replication	Stim x Genotype F(10,88)=3.473 Stim F(2,88)=13.74 Genotype F(5,44)=1.115	Stim x Genotype P=0.0007 Stim P<0.0001 Genotype P=0.3663	Pre vs LaserON | Pre vs LaserOFF | LaserON vs LaserOFF : D1/D2: P=0.1548 | P=0.1830 | P=0.9958 D1: P<0.0001 | P=0.9701 | P<0.0001 D2: P=0.0339 | P=0.0809 | P=0.9293 D1+D1/D2: P=0.0004 | P=0.9097 | P=0.0015 D2+D1/D2: P=0.9211 | P=0.6253| P=0.8520 D1/D2^{ctl}: P=0.9791 | P=0.8612 | P=0.7539
Extended Data Figure 4a (right) Bout mean duration Locomotion	D1/D2: 13 mice D1: 11 mice D2: 8 mice D1+D1/D2: 6 mice D2+D1/D2: 5 mice D1/D2^{ctl}: 7 mice	2-way ANOVA with one factor replication	Stim x Genotype F(10,88)=3.695 Stim F(2,88)=7.636 Genotype F(5,44)=3.009	Stim x Genotype P=0.0004 Stim P=0.0009 Genotype P=0.0202	Pre vs LaserON | Pre vs LaserOFF | LaserON vs LaserOFF : D1/D2: P=0.4854 | P=0.2390 | P=0.8821 D1: P=0.3577 | P=0.1294 | P=0.0036 D2: P=0.0577 | P=0.4866 | P=0.0023 D1+D1/D2: P=0.0003 | P=0.9297 | P<0.00001 D2+D1/D2: P=0.9703 | P=0.2754 | P=0.1829 D1/D2^{ctl}: P=0.8223 | P=0.6978 | P=0.9752
Extended Data Figure 4b (middle) Bout number Small movements	D1/D2: 13 mice D1: 11 mice D2: 8 mice D1+D1/D2: 6 mice D2+D1/D2: 5 mice D1/D2^{ctl}: 7 mice	2-way ANOVA with one factor replication	Stim x Genotype F(10,88)=9.386 Stim F(2,88)=172.1 Genotype F(5,44)=5.558	Stim x Genotype P<0.0001 Stim P<0.0001 Genotype P=0.0005	Pre vs LaserON | Pre vs LaserOFF | LaserON vs LaserOFF : D1/D2: P<0.0001 | P=0.9254 | P<0.0001 D1: P<0.0001 | P=0.6216 | P<0.0001 D2: P<0.0001 | P=0.4554 | P<0.0001 D1+D1/D2: P<0.0001 | P=0.9682 | P<0.0001 D2+D1/D2: P<0.0001 | P=0.4660 | P<0.0001 D1/D2^{ctl}: P=0.9571 | P=0.8872 | P=0.9815
Extended Data Figure 4b (right) Bout mean duration Small movements	D1/D2: 13 mice D1: 11 mice D2: 8 mice D1+D1/D2: 6 mice D2+D1/D2: 5 mice D1/D2^{ctl}: 7 mice	2-way ANOVA with one factor replication	Stim x Genotype F(10,88)=39.47 Stim F(2,88)=0.3315 Genotype F(5,44)=10.98	Stim x Genotype P<0.0001 Stim P=0.7187 Genotype P<0.0001	Pre vs LaserON | Pre vs LaserOFF | LaserON vs LaserOFF : D1/D2: P<0.0001 | P=8294 | P<0.0001 D1: P<0.0001 | P=0.6568 | P<0.0001 D2: P<0.0001 | P=0.7507 | P<0.0001 D1+D1/D2: P<0.0001 | P=0.7803 | P=0.0001 D2+D1/D2: P<0.0001 | P=0.9313 | P<0.0001 D1/D2^{ctl}: P=0.5418 | P=0.9975 | P=0.2295
Extended Data Figure 4c (middle) Bout number Immobility	D1/D2: 13 mice D1: 11 mice D2: 8 mice D1+D1/D2: 6 mice D2+D1/D2: 5 mice D1/D2^{ctl}: 7 mice	2-way ANOVA with one factor replication	Stim x Genotype F(10,88)=29.95 Stim F(2,88)=17.82 Genotype F(5,44)=8.523	Stim x Genotype P<0.0001 Stim P<0.0001 Genotype P<0.0001	Pre vs LaserON | Pre vs LaserOFF | LaserON vs LaserOFF : D1/D2: P<0.0001 | P=0.0364 | P<0.0001 D1: P<0.0001 | P=0.0345 | P<0.0001 D2: P<0.0001 | P=0.2474 | P<0.0001 D1+D1/D2: P=0.0001 | P=0.9862 | P<0.0001 D2+D1/D2: P<0.0001 | P=0.3821 | P<0.0001 D1/D2^{ctl}: P=0.2295 | P=0.9785 | P=0.3182
Extended Data Figure 4c (right) Bout mean duration Immobility	D1/D2: 13 mice D1: 11 mice D2: 8 mice D1+D1/D2: 6 mice D2+D1/D2: 5 mice D1/D2^{ctl}: 7 mice	2-way ANOVA with one factor replication	Stim x Genotype F(10,88)=5.886 Stim F(2,88)=9.378 Genotype F(5,44)=5.973	Stim x Genotype P<0.0001 Stim P=0.0002 Genotype P=0.0003	Pre vs LaserON | Pre vs LaserOFF | LaserON vs LaserOFF : D1/D2: P<0.0001 | P=0.2911 | P=0.0002 D1: P=0.6011 | P=0.1980 | P=0.0224 D2: P<0.0001 | P=0.025 | P=0.0694 D1+D1/D2: P=0.3897 | P=0.2025 | P=0.0087 D2+D1/D2: P=0.0350 | P=0.8386 | P=0.1276 D1/D2^{ctl}: P=0.9799 | P=0.1612 | P=0.1095
Extended Data Figure 4f	D1/D2: 13 mice D1: 11 mice D2: 8 mice D1+D1/D2: 6 mice D2+D1/D2: 5 mice D1/D2^{ctl}: 7 mice	3-way ANOVA with two factors (time, stim) replication	Genotype F(5,44)=1.50 Time F(60,2640)=595.78 Geno x time F(300,2640)=4.86 Stim F(2,88)=18.09 Geno x stim F(10,88)=0.778 Time x stim F(120,5280)=21.77 Geno x time x stim F(600,5280)=8.82	Genotype P=0.295 Time P=1.6e-106 Geno x time P=9.5e-10 Stim P=1.57e-6 Geno x stim P=0.649 Time x stim P=3.1e-29 Geno x time x stim P=2.3e-36	Difference with D1/D2 during the first second after locomotion onset D1: p<0.0001 D2: p=0.010 D1 + D1/D2: p<0.0001 D2 + D1/D2: p=0.328 D1/D2^{ctl}: p=0.0424
Figure 4c Extended Data Figure 5 L>L	D1: 11 mice D2: 8 mice D1+D1/D2: 6 mice D2+D1/D2: 5 mice D1/D2: 13 mice D1/D2^{ctl}: 7 mice	2-way ANOVA with one factor replication	Stim x Genotype F(10,88)=3.876 Stim F(2,88)=17.36 Genotype F(5,44)=3.212	Stim x Genotype P=0.0002 Stim P<0.0001 Genotype P=0.0148	Pre vs LaserON | Pre vs LaserOFF | LaserON vs LaserOFF : D1/D2: P=0.8932 | P=0.0804 | P=0.2012 D1: P=0.0080 | P=0.0378 | P<0.0001 D2: P=0.0011 | P=0.3250 | P<0.0001 D1+D1/D2: P=0.0060 | P=0.9290 | P=0.0019 D2+D1/D2: P=0.8461 | P=0.1988 | P=0.4672 D1/D2^{ctl}: P=0.9947 | P=0.7233 | P=0.7816
Figure 4c Extended Data Figure 5 L>S	D1: 11 mice D2: 8 mice D1+D1/D2: 6 mice D2+D1/D2: 5 mice	2-way ANOVA with one factor replication	Stim x Genotype F(10,88)=11.48 Stim F(2,88)=123.0	Stim x Genotype P<0.0001 Stim P<0.0001	Pre vs LaserON | Pre vs LaserOFF | LaserON vs LaserOFF : D1/D2: P<0.0001 | P=0.0377 | P<0.0001 D1: P=0.0636 | P=0.1269 | P=0.0002 D2: P<0.0001 | P=0.3258 | P<0.0001

	D1/D2: 13 mice D1/D2^{ctl}: 7 mice		Genotype F(5,44)=2.975	Genotype P=0.0213	D1+D1/D2: P<0.0001 | P=0.1838 | P<0.0001 D2+D1/D2: P<0.0001 | P=0.1838 | P<0.0001 D1/D2^{ctl}: P=0.9194 | P=0.7655 | P=0.5238
Figure 4c Extended Data Figure 5 L>I	D1: 11 mice D2: 8 mice D1+D1/D2: 6 mice D2+D1/D2: 5 mice D1/D2: 13 mice D1/D2^{ctl}: 7 mice	2-way ANOVA with one factor replication	Stim x Genotype F(10,88)=33.09 Stim F(2,88)=88.43 Genotype F(5,44)=24.94	Stim x Genotype P<0.0001 Stim P<0.0001 Genotype P<0.0001	Pre vs LaserON | Pre vs LaserOFF | LaserON vs LaserOFF : D1/D2: P<0.0001 | P=0.9571 | P<0.0001 D1: P=0.0624 | P=0.2100 | P=0.0004 D2: P<0.0001 | P=0.8650 | P<0.0001 D1+D1/D2: P=0.3529 | P=0.9928 | P=0.2959 D2+D1/D2: P<0.0001 | P=0.8469 | P<0.0001 D1/D2^{ctl}: P=0.7134 | P=0.9232 | P=0.9142
Figure 4c Extended Data Figure 5 S>L	D1: 11 mice D2: 8 mice D1+D1/D2: 6 mice D2+D1/D2: 5 mice D1/D2: 13 mice D1/D2^{ctl}: 7 mice	2-way ANOVA with one factor replication	Stim x Genotype F(10,88)=19.31 Stim F(2,88)=23.85 Genotype F(5,44)=5.40	Stim x Genotype P<0.0001 Stim P<0.0001 Genotype P=0.0006	Pre vs LaserON | Pre vs LaserOFF | LaserON vs LaserOFF : D1/D2: P<0.0001 | P=0.0703 | P<0.0001 D1: P<0.0001 | P=0.8816 | P<0.0001 D2: P<0.0001 | P=0.1062 | P<0.0001 D1+D1/D2: P=0.3762 | P=0.7394 | P=0.0992 D2+D1/D2: P<0.0001 | P=0.8231 | P<0.0001 D1/D2^{ctl}: P=0.9739 | P=0.9376 | P=0.6409
Figure 4c Extended Data Figure 5 S>S	D1: 11 mice D2: 8 mice D1+D1/D2: 6 mice D2+D1/D2: 5 mice D1/D2: 13 mice D1/D2^{ctl}: 7 mice	2-way ANOVA with one factor replication	Stim x Genotype F(10,88)=56.73 Stim F(2,88)=59.23 Genotype F(5,44)=15.00	Stim x Genotype P<0.0001 Stim P<0.0001 Genotype P<0.0001	Pre vs LaserON | Pre vs LaserOFF | LaserON vs LaserOFF : D1/D2: P<0.0001 | P=0.5490 | P<0.0001 D1: P<0.0001 | P=0.7355 | P<0.0001 D2: P<0.0001 | P=0.5342 | P<0.0001 D1+D1/D2: P=0.0017 | P=0.6400 | P<0.0001 D2+D1/D2: P<0.0001 | P=0.9967 | P<0.0001 D1/D2^{ctl}: P=0.6850 | P=0.9824 | P=0.5723
Figure 4c Extended Data Figure 5 S>I	D1: 11 mice D2: 8 mice D1+D1/D2: 6 mice D2+D1/D2: 5 mice D1/D2: 13 mice D1/D2^{ctl}: 7 mice	2-way ANOVA with one factor replication	Stim x Genotype F(10,88)=31.73 Stim F(2,88)=25.72 Genotype F(5,44)=14.95	Stim x Genotype P<0.0001 Stim P<0.0001 Genotype P<0.0001	Pre vs LaserON | Pre vs LaserOFF | LaserON vs LaserOFF : D1/D2: P<0.0001 | P=0.1822 | P<0.0001 D1: P<0.0001 | P=0.1318 | P<0.0001 D2: P<0.0001 | P=0.3196 | P<0.0001 D1+D1/D2: P=0.0013 | P=0.9499 | P=0.0004 D2+D1/D2: P<0.0001 | P=0.7058 | P<0.0001 D1/D2^{ctl}: P=0.5798 | P=0.9686 | P=0.7296
Figure 4c Extended Data Figure 5 I>L	D1: 11 mice D2: 8 mice D1+D1/D2: 6 mice D2+D1/D2: 5 mice D1/D2: 13 mice D1/D2^{ctl}: 7 mice	2-way ANOVA with one factor replication	Stim x Genotype F(10,88)=5.22 Stim F(2,88)=4.40 Genotype F(5,44)=1.73	Stim x Genotype P<0.0001 Stim P=0.0151 Genotype P=0.1468	Pre vs LaserON | Pre vs LaserOFF | LaserON vs LaserOFF : D1/D2: P=0.1783 | P=0.3399 | P=0.0053 D1: P=0.0002 | P=0.5738 | P=0.0062 D2: P=0.0153 | P=0.6668 | P=0.0011 D1+D1/D2: P=0.0213 | P=0.5088 | P=0.2486 D2+D1/D2: P=0.5716 | P=0.3772 | P=0.0541 D1/D2^{ctl}: P=0.4047 | P=0.8444 | P=0.1613
Figure 4c Extended Data Figure 5 I>S	D1: 11 mice D2: 8 mice D1+D1/D2: 6 mice D2+D1/D2: 5 mice D1/D2: 13 mice D1/D2^{ctl}: 7 mice	2-way ANOVA with one factor replication	Stim x Genotype F(10,88)=19.43 Stim F(2,88)=3.968 Genotype F(5,44)=14.93	Stim x Genotype P<0.0001 Stim P=0.0224 Genotype P<0.0001	Pre vs LaserON | Pre vs LaserOFF | LaserON vs LaserOFF : D1/D2: P<0.0001 | P=0.3976 | P<0.0001 D1: P<0.0001 | P=0.1824 | P<0.0001 D2: P<0.0001 | P=0.3864 | P=0.0005 D1+D1/D2: P=0.0016 | P=0.2473 | P<0.0001 D2+D1/D2: P=0.0004 | P=0.9442 | P<0.0001 D1/D2^{ctl}: P=0.8611 | P=0.9159 | P=0.9918
Figure 4c Extended Data Figure 5 I>I	D1: 11 mice D2: 8 mice D1+D1/D2: 6 mice D2+D1/D2: 5 mice D1/D2: 13 mice D1/D2^{ctl}: 7 mice	2-way ANOVA with one factor replication	Stim x Genotype F(10,88)=7.142 Stim F(2,88)=5.197 Genotype F(5,44)=6.965	Stim x Genotype P<0.0001 Stim P=0.0074 Genotype P<0.0001	Pre vs LaserON | Pre vs LaserOFF | LaserON vs LaserOFF : D1/D2: P<0.0001 | P=0.1769 | P=0.0105 D1: P=0.0042 | P=0.1182 | P<0.0001 D2: P=0.0092 | P=0.2768 | P=0.3058 D1+D1/D2: P=0.2151 | P=0.1426 | P=0.0015 D2+D1/D2: P=0.0146 | P=0.9203 | P=0.0406 D1/D2^{ctl}: P=0.9790 | P=0.8146 | P=0.6997
Figure 5c	D1/D2: 11 cells D1: 9 cells D2: 8 cells	2-way ANOVA with one factor replication	Geno F(2,25)=61.9 Drug F(1,25)=37.5 Geno x drug F(2,25)=165.2	Geno P=0.054 Drug P=0.032 Geno x drug P=2.3e-6	D1 base vs drug: P=0.008 D2 base vs drug: P=0.005 D1/D2 base vs drug: P=0.0002 Drug effect D1 vs D2: P=9.5e-5 Drug effect D1 vs D1/D2: P=0.96 Drug effect D2 vs D1/D2: P=2.3e-5
Figure 5d	D1/D2: 11 cells D1: 9 cells D2: 8 cells	2-way ANOVA with one factor replication	Geno F(2,25)=2.9 Drug F(1,25)=19.9 Geno x drug F(2,25)=39.8	Geno P=0.072 Drug P=0.0002 Geno x drug P=1.7e-8	D1 base vs drug: P=6.8e-6 D2 base vs drug: P=0.02 D1/D2 base vs drug: P=0.08 Drug effect D1 vs D2: P=3.7e-7 Drug effect D1 vs D1/D2: P=1.8e-5 Drug effect D2 vs D1/D2: P=0.002
Figure 5e	D1/D2: 10 cells D1: 9 cells D2: 7 cells	2-way ANOVA with one factor replication	Geno F(2,23)=3.5 Drug F(1,23)=1.2 Geno x drug F(2,23)=8.22	Geno P=0.046 Drug P=0.28 Geno x drug P=0.002	D1 base vs drug: P=0.36 D2 base vs drug: P=0.08 D1/D2 base vs drug: P=0.005 Drug effect D1 vs D2: P=0.17 Drug effect D1 vs D1/D2: P=0.007 Drug effect D2 vs D1/D2: P=0.008
Figure 5f	D1/D2: 12 cells D1: 5 cells D2: 6 cells	2-way ANOVA with one factor replication	Geno F(2,20)=0.1 Drug F(1,20)=13.0 Geno x drug F(2,20)=18.4	Geno P=0.90 Drug P=0.002 Geno x drug P=2.6e-5	D1 base vs drug: P=0.0004 D2 base vs drug: P=0.026 D1/D2 base vs drug: P=0.007 Drug effect D1 vs D2: P=0.38 Drug effect D1 vs D1/D2: P=1.6e-6 Drug effect D2 vs D1/D2: P=0.0045
Figure 5g	D1/D2: 12 cells D1: 5 cells D2: 6 cells	2-way ANOVA with one factor replication	Geno F(2,20)=0.58 Drug F(1,20)=5.8 Geno x drug F(2,20)=6.3	Geno P=0.57 Drug P=0.026 Geno x drug P=0.007	D1 base vs drug: P=3.5e-6 D2 base vs drug: P=0.22 D1/D2 base vs drug: P=0.40 Drug effect D1 vs D2: P=0.006 Drug effect D1 vs D1/D2: P=0.0003

					Drug effect D2 vs D1/D2: P=0.14
Extended Data Figure 6c	D1/D2: 12 cells D1: 9 cells D2: 7 cells	2-way ANOVA with one factor replication	Geno F(2,23)=2.80 Drug F(1,23)=0.05 Geno x drug F(2,23)=7.66	Geno P=0.08 Drug P=0.82 Geno x drug P=0.0028	D1 base vs drug: P=0.041 D2 base vs drug: P=0.021 D1/D2 base vs drug: P=0.48 Drug effect D1 vs D2: P=0.002 Drug effect D1 vs D1/D2: P=0.029 Drug effect D2 vs D1/D2: P=0.059
Extended Data Figure 6d	D1/D2: 10 cells D1: 9 cells D2: 8 cells	2-way ANOVA with one factor replication	Geno F(2,24)=0.38 Drug F(1,24)=13.4 Geno x drug F(2,23)=23.8	Geno P=0.69 Drug P=0.0012 Geno x drug P=2.0e-6	D1 base vs drug: P=0.0004 D2 base vs drug: P=0.032 D1/D2 base vs drug: P=0.0002 Drug effect D1 vs D2: P=5.7e-5 Drug effect D1 vs D1/D2: P=0.08 Drug effect D2 vs D1/D2: P=0.0005
Extended Data Figure 6e	D1/D2: 11 cells D1: 5 cells D2: 8 cells	3-way ANOVA with two factors replication	Geno F(2,21)=3.25 Frequency F(16,336)=96.0 Geno x freq F(32,336)=3.41 Drug F(1,21)=92;6 Geno x drug F(2,21)=163.4 Freq x drug F(16,336)=22.8 Geno x freq x drug F(32,336)=30.7	Geno: P=0.059 Frequency: P<1e-12 Geno x freq: P=1e-8 Drug: P=3.8e-9 Geno x drug: P<1e-12 Freq x drug: P<1e-12 Geno x freq x drug: P<1e-12	
Extended Data Figure 6f	D1/D2-SPNs D1R antago: 5 D2R antago: 5	2-way ANOVA with one factor replication	Antago F(1,8)=1.38 Drug F(1,8)=8.43 Antago x drug F(1,8)=9.62	Antago: P=0.27 Drug: P=0.020 Antago x drug: P=0.015	D1R antago: P=0.87 D2R antago: P=0.021 Antago effect D1R vs D2R: P=0.016
Extended Data Figure 6g	D1/D2-SPNs D1R antago: 5 D2R antago: 5	2-way ANOVA with one factor replication	Antago F(1,8)=0.05 Drug F(1,8)=41.1 Antago x drug F(1,8)=8.94	Antago: P=0.82 Drug: P=0.0002 Geno x drug: P=0.017	D1R antago: P=0.12 D2R antago: P=0.0007 Antago effect D1R vs D2R: P=0.022
Extended Data Figure 6h	D1/D2-SPNs No antago: 11 D1R antago: 5 D2R antago: 5	2-way ANOVA with one factor replication	Antago F(2,18)=2.04 Drug F(1,18)=18.01 Antago x drug F(2,18)=7.32	Antago: P=0.16 Drug: P=0.0005 Antago x drug: P=0.0047	No antago base vs drug: P=0.0002 D1R antago base vs drug: P=0.37 D2R antago base vs drug: P=0.048 Drug effect no antago vs D1R antago: P=0.0003 Drug effect no antago vs D2R antago: P=0.67 Drug effect D1R antago vs D2R antago: P=0.029
Extended Data Figure 6i	D1/D2-SPNs No antago: 11 D1R antago: 5 D2R antago: 5	2-way ANOVA with one factor replication	Antago F(2,18)=0.97 Drug F(1,18)=0.81 Antago x drug F(2,18)=1.73	Antago: P=0.40 Drug: P=0.38 Antago x drug: P=0.21	No antago base vs drug: P=0.08 D1R antago base vs drug: P=0.09 D2R antago base vs drug: P=0.57 Drug effect no antago vs D1R antago: P=0.021 Drug effect no antago vs D2R antago: P=0.51 Drug effect D1R antago vs D2R antago: P=0.265
Extended Data Figure 6j	D1/D2-SPNs No antago: 10 D1R antago: 5 D2R antago: 5	2-way ANOVA with one factor replication	Antago F(2,17)=2.34 Drug F(1,17)=14.40 Antago x drug F(2,17)=2.47	Antago: P=0.13 Drug: P=0.0015 Antago x drug: P=0.11	No antago base vs drug: P=0.005 D1R antago base vs drug: P=0.208 D2R antago base vs drug: P=0.0298 Drug effect no antago vs D1R antago: P=0.018 Drug effect no antago vs D2R antago: P=0.29 Drug effect D1R antago vs D2R antago: P=0.087
Extended Data Figure 6l	D1/D2-SPNs No antago: 10 D1R antago: 5 D2R antago: 5	2-way ANOVA with one factor replication	Antago F(2,17)=0.45 Drug F(1,17)=0.04 Antago x drug F(2,17)=3.56	Antago: P=0.64 Drug: P=0.83 Antago x drug: P=0.049	No antago base vs drug: P=0.007 D1R antago base vs drug: P=0.41 D2R antago base vs drug: P=0.69 Drug effect no antago vs D1R antago: P=0.047 Drug effect no antago vs D2R antago: P=0.16 Drug effect D1R antago vs D2R antago: P=0.85
Extended Data Figure 6m	D1/D2-SPNs No antago: 10 D1R antago: 5 D2R antago: 5	2-way ANOVA with one factor replication	Antago F(2,17)=1.25 Drug F(1,17)=0.30 Antago x drug F(2,17)=1.15	Antago: P=0.30 Drug: P=0.59 Antago x drug: P=0.34	No antago base vs drug: P=0.39 D1R antago base vs drug: P=0.37 D2R antago base vs drug: P=0.20 Drug effect no antago vs D1R antago: P=0.21 Drug effect no antago vs D2R antago: P=0.13 Drug effect D1R antago vs D2R antago: P=0.96
Figure 6c-d	NaCl : $D1^{WT}$/D2: 18 $D1^{cKO}$/D2: 18 1 mg/kg : $D1^{WT}$/D2: 18 $D1^{cKO}$/D2: 18 5 mg/kg : $D1^{WT}$/D2: 14 $D1^{cKO}$/D2: 14 10 mg/kg: $D1^{WT}$/D2: 8 $D1^{cKO}$/D2: 8 20 mg/kg : $D1^{WT}$/D2: 8 $D1^{cKO}$/D2: 8	3-way ANOVA with one factor (time) replication	Genotype F(1,122)=51.01 Dose F(4,122)=14.32 Geno x Dose F(4,122)=2.48 Time F(23,2806)=33.30 Geno x Time F(23,2806)=7.51 Dose x Time F(92,2806)=2.77 Geno x Dose x Time F(92,2806)=1.99	Genotype P=7.3e-11 Dose P=1.3e-9 Geno x Dose P=0.048 Time P=1.8e-30 Geno x Time P=6.3e-7 Dose x Time P=5.6e-5 Geno x Dose x Time P=0.0062	$D1^{WT}$/D2 vs $D1^{cKO}$/D2 temporal evolution of distance NaCl: P=0.037 1 mg/kg: P=0.017 5 mg/kg: P=0.013 10 mg/kg: P<0.0001 20 mg/kg: P=0.001 $D1^{WT}$/D2 vs $D1^{cKO}$/D2 total distance NaCl: P=0.012 1 mg/kg: P<0.0001 5 mg/kg: P=0.0002 10 mg/kg: P<0.0001 20 mg/kg: P=0.346 total distance vs NaCl 1 mg/kg: $D1^{WT}$/D2 P=0.986 $D1^{cKO}$/D2 P=0.089 5 mg/kg: $D1^{WT}$/D2 P=0.699 $D1^{cKO}$/D2 P=0.0276 10 mg/kg: $D1^{WT}$/D2 P=0.186 $D1^{cKO}$/D2 P<0.0001 20 mg/kg: $D1^{WT}$/D2 P<0.0001 $D1^{cKO}$/D2 P=0.0007
Figure 6e Extended Data Figure 7b	$D1^{WT}$/D2: 17 $D1^{cKO}$/D2: 16	3-way ANOVA with two factors (time, days) replication	Genotype F(1,31)=9.63 Time F(26,806)=37.47 Geno x Time F(26,806)=8.36 Days F(6,186)=1.32 Geno x Days F(6,186)=3.79	Genotype P=0.0004 Time P<0.0001 Geno x Time P=0.0002 Days P=0.271 Geno x Days P=0.0121 Days x Time P<0.0001	$D1^{WT}$/D2 vs $D1^{cKO}$/D2 temporal evolution of distance Day 1: P<0.0001 Day 2: P<0.0001 Day 3: P<0.0001 Day 4: P<0.0001 Day 5: P<0.0001 Day 6: P<0.0001

			Days x Time F(156,4836)=4.32 Geno x Days x Time F(156,4836)=1.45	Geno x Days x Time P=0.125	Day 14: P<0.0001 effect of days $D1^{WT}$/D2: P<0.0001 $D1^{cKO}$/D2 P=0.387 total distance vs Day 1 Day 2: $D1^{WT}$/D2 P=0.5391 $D1^{cKO}$/D2 P=0.632 Day 3: $D1^{WT}$/D2 P=0.0101 $D1^{cKO}$/D2 P=0.993 Day 4: $D1^{WT}$/D2 P=0.0043 $D1^{cKO}$/D2 P=0.999 Day 5: $D1^{WT}$/D2 P<0.0001 $D1^{cKO}$/D2 P=0.748 Day 6: $D1^{WT}$/D2 P<0.0001 $D1^{cKO}$/D2 P=0.879 Day 17: $D1^{WT}$/D2 P=0.0005 $D1^{cKO}$/D2 P=0.908
Figure 6f	$D1^{WT}$/D2: 12 $D1^{cKO}$/D2: 9	2-way ANOVA with one factor replication	Drug dose x Genotype F(1,19)=1.10 Drug F(1,19)=31.03 Genotype F(1,19)=1.74	Drug dose x Genotype P=0.308 Drug Dose P<0.0001 Genotype P=0.203	$D1^{WT}$/D2 vs $D1^{cKO}$/D2 NaCl: P=0.830 10 mg/kg: P=0.297
Extended Data Figure 7a	NaCl : $D1^{WT}$/D2: 8 $D1^{cKO}$/D2: 6 1 mg/kg : $D1^{WT}$/D2: 8 $D1^{cKO}$/D2: 8 3 mg/kg : $D1^{WT}$/D2: 7 $D1^{cKO}$/D2: 7	3-way ANOVA with one factor replication	Genotype F(1,34)=8.03 Dose F(2,34)=35.83 Geno x Dose F(2,342)=0.39 Time F(23,782)=20.02 Geno x Time F(23,782)=3.12 Dose x Time F(46,782)=9.81 Geno x Dose x Time F(46,782)=1.75	Genotype P=0.0077 Dose P=4.3e-9 Geno x Dose P=0.681 Time P=3.7e-15 Geno x Time P=0.0113 Dose x Time P=1.9e-12 Geno x Dose x Time P=0.0763	$D1^{WT}$/D2 vs $D1^{cKO}$/D2 temporal evolution of distance NaCl: P=0.009 1 mg/kg: P<0.0001 3 mg/kg: P=0.947 $D1^{WT}$/D2 vs $D1^{cKO}$/D2 total distance over 60 min NaCl: P<0.0001 1 mg/kg: P=0.015 3 mg/kg: P=0.710

Unexpected inhibition of motor function by dopamine activation of D1/D2 co-expressing striatal neurons.

Patricia Bonnavion†, Christophe Varin†, Ghazal Fakhfouri, Aurélie De Groote, Amandine Cornil, Elsa Isingrini, Quentin Rainer, Kathleen Xu, Eleni Tzavara, Erika Vigneault, Sylvie Dumas, Alban de Kerchove d'Exaerde* and Bruno Giros*

EF 1: Anatomical characterization of D1/D2-SPNs and generation and validation of a novel $D1^{FlpO}/A2a^{Cre}$ transgenic line.

EF 2: Electrophysiological characterization of the three SPNs subpopulations.

EF 3: Ex vivo and histological controls for optogenetic experiments

EF 4: Architecture of motor states and locomotion velocity during optogenetic stimulation.

EF 5: Temporal organization of motor states.

EF 6: Effects of DA application on SPNs subpopulations.

EF 7: Supplements on the phenotypic characterization of $D1^{cKO}$/D2 mice

EF 8: Proposed model of integration of D1/D2-SPNs into striatal physiology.

Extended Data Table 1: Complete list of electrophysiological properties recorded in D1/D2-, D1- and D2-SPNs.

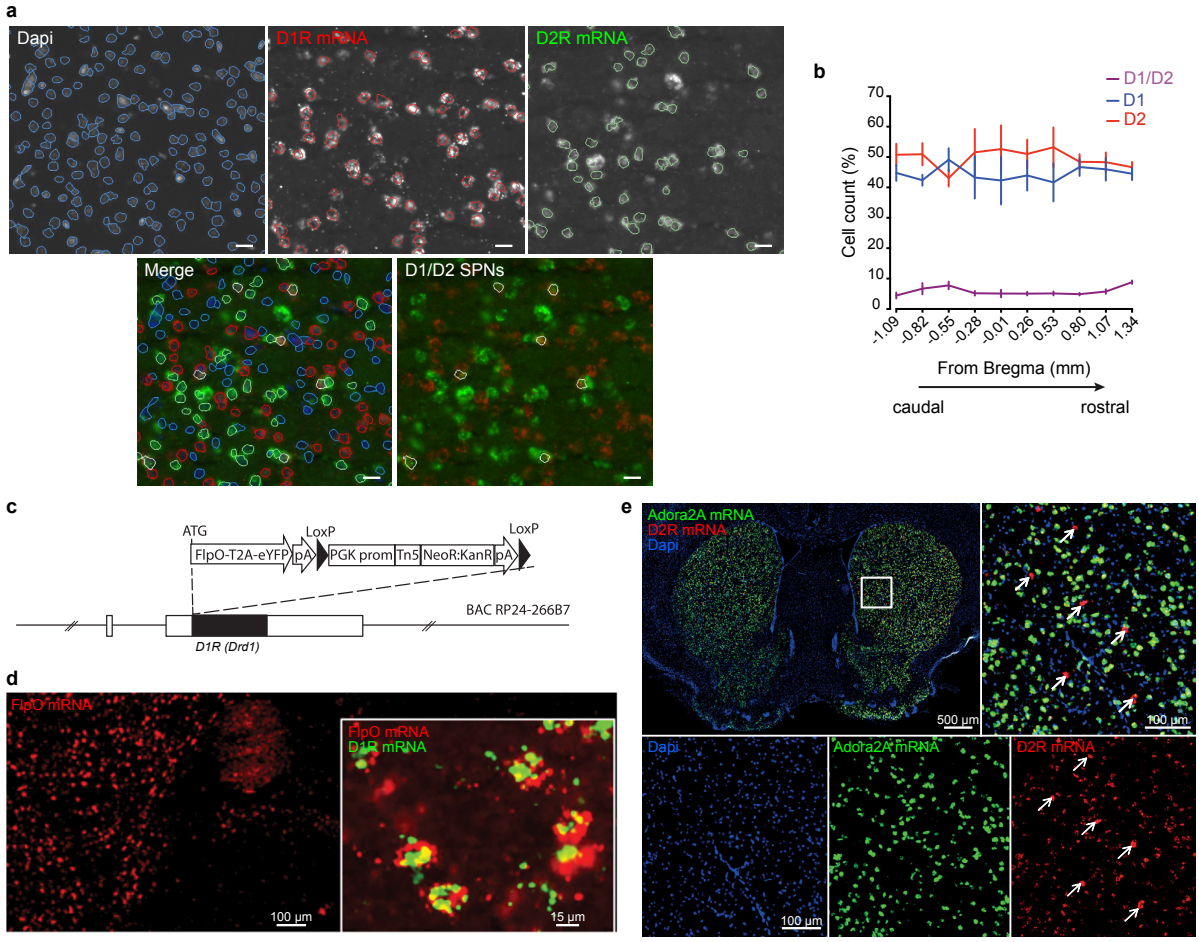

Extended Data Figure 1. Anatomical characterization of D1/D2-SPNs and generation and validation of a novel D1^{FlpO}/A2a^{Cre} transgenic line.

a, Representative coronal section in the dorsal striatum illustrating fluorescent in situ hybridization of D1R and D2R mRNAs and Dapi staining. Using a CellProfiler pipeline, segmentation was first performed on dapi staining to outline all cells (blue contours). Then D1- and D2-posivive cells are identified using an intensity threshold in red and green channels, respectively (red and green contours). Scale: 20 µm. **b**, Quantification of D1-, D2-, and D1/D2-positive cells throughout the rostro-caudal extent of the dorsal striatum (n = 3 mice). **c**, Diagram illustrating the generation of D1^{FlpO} mice. **d**, Photomicrograph of a coronal brain section at the level of the dorsal striatum after in situ hybridization of FlpO (red) and D1R (green) mRNAs illustrating expression of FlpO-recombinase in D1-expressing SPNs. **e**, Coronal brain section after in situ hybridization of D2R (green) and Adora2A (red) mRNAs counterstained with dapi (blue) illustrating specific expression of AdoraA2 in D2-SPNs[34]. Some cells expressing D2R and not AdoraA2 (arrows) correspond to cholinergic interneurons.

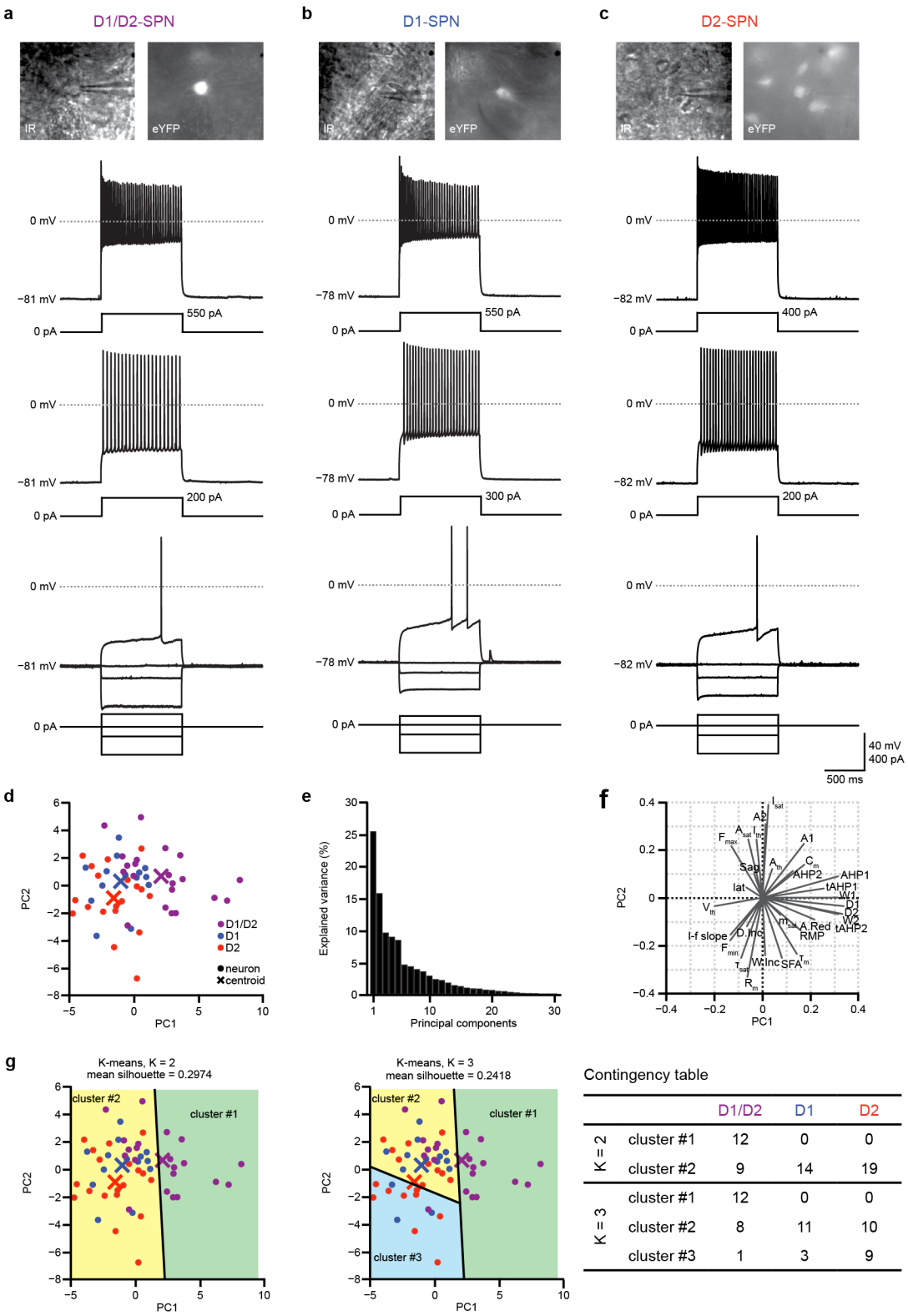

Contingency table

		D1/D2	D1	D2
K = 2	cluster #1	12	0	0
	cluster #2	9	14	19
K = 3	cluster #1	12	0	0
	cluster #2	8	11	10
	cluster #3	1	3	9

Extended Data Figure 2. Electrophysiological characterization of the three SPNs subpopulations.a-c, Representative example of voltage response to current steps in one D1/D2-SPN (**a**), one D1-SPN (**b**) and one D2-SPN (**c**), with their corresponding photomicrograph under infrared illumination (IR, top left) and under fluorescent illumination (eYFP, top right). **d**, Two-dimensional projection of the set of neurons recorded following PCA into the first- and second-order components. Individual cells are represented in violet (D1/D2), blue (D1) and red (D2) circles; crosses represent centroids of D1/D2-SPNs (violet), D1-SPNs (blue) and D2-SPNs (red). **e**, Percent of variance explained as a function of the number of principal components. **f**, Two-dimensional projection of orthonormal principal component coefficients for each parameter. (*Abbreviations: RMP: resting membrane*

potential; R_m: input membrane resistance; τ_m: membrane time constant; C_m: membrane capacitance; Sag: Sag index; I_{th}: step intensity to first spike; lat: first spike latency; V_{th}: action potential; A_{th}: adaptation around threshold; F_{min}: minimal steady state frequency around threshold; I–f slope: early slope of the current-frequency relationship; I_{sat}: step intensity to saturation; A_{sat}: amplitude of early adaptation at high firing; τ_{sat}: time constant of early adaptation at high firing; m_{sat}: slope of late adaptation at high firing; F_{max}: maximal steady state frequency at high firing; SFA: spike frequency adaptation at high firing; A1: amplitude of the first action potential; A2: amplitude of the second action potential; D1: duration of the first action potential; D2: duration of the second action potential; W1: spike half-widths of the first action potential; W2: spike half-widths of the second action potential; AHP1: AHP maximum of the first action potential; AHP2: AHP potential maximum of the second action potential; tAHP1: AHP latency after of the first action potential; tAHP2: AHP latency of the second action potential; A.Red: amplitude reduction; D.Inc: duration increase; W.Inc: half-width duration increase). **g**, Clusters obtained after k-means partitioning (left, k = 2; middle, k = 3) based on all the electrophysiological parameters recorded, and contingency table (right) comparing clusters assignments (lines) and cell identity defined by INTRSECT eYFP labelling.

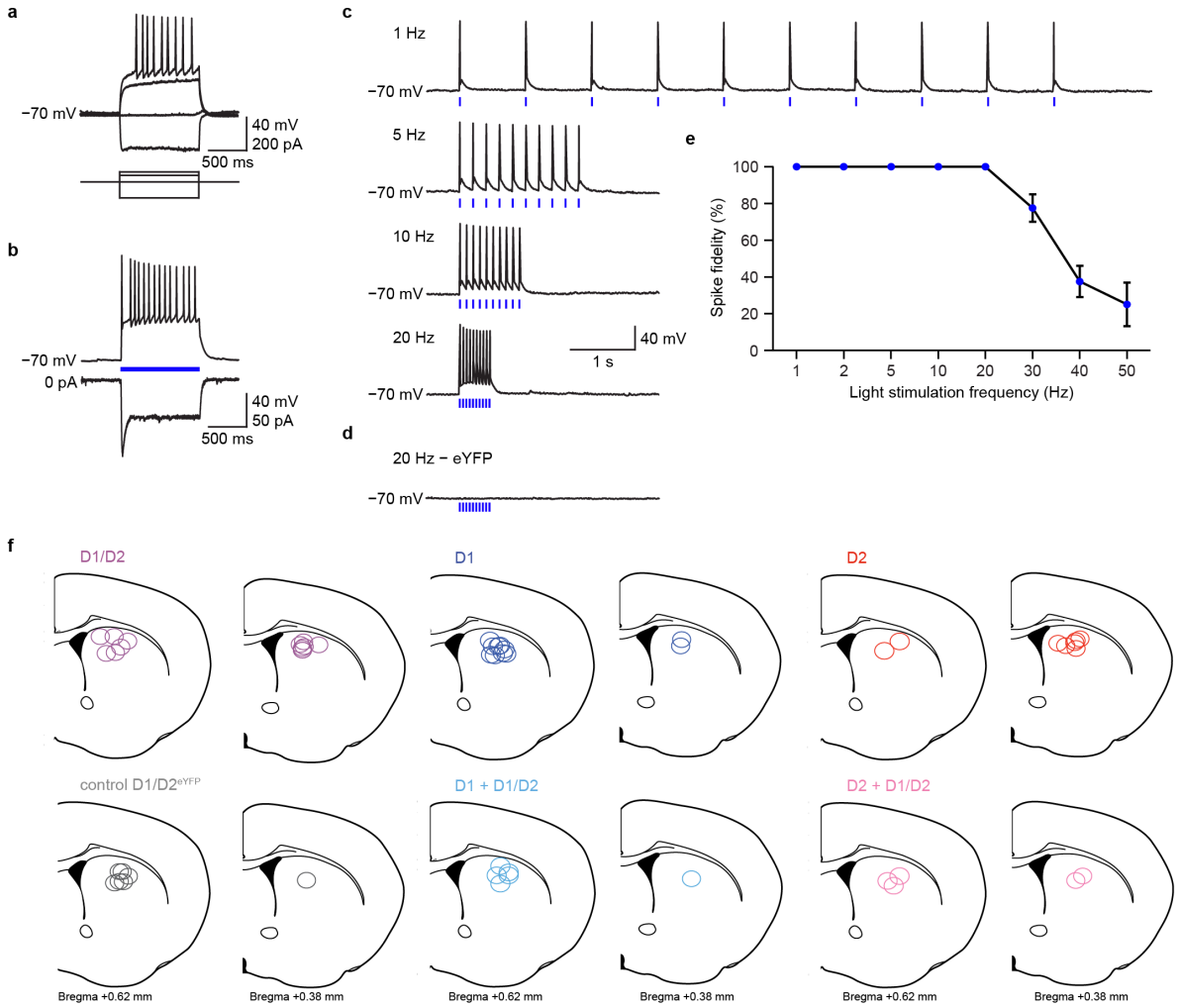

Extended Data Figure 3. Ex vivo and histological controls for optogenetic experiments. a, Voltage response of an eYFP-expressing D1/D2-SPN to hyperpolarizing and depolarizing current injection displaying the typical features of SPNs. **b**, ChR2-expressing SPN (same as in A) displays robust depolarization and firing activity in response to a 1 s blue light illumination when recorded in current-clamp mode (top), and an inward current when recorded in voltage-clamp mode (bottom). **c**, Representative example of the same D1/D2-SPN depicted in **a** illustrating that pulses of light (5 ms) faithfully elicited spikes for frequencies up to 20 Hz. **d**, In a D1/D2-SPN only expressing eYFP, light stimulation is inefficient. **e**, Spike fidelity in response to light pulses at different frequencies (1-50 Hz) (n = 4 cells from 3 different mice). **f**, Schematic representation of the position of the tip of the optic fiber after histological control for all experimental groups (D1/D2, n = 13; control D1/D2^{eYFP}, n = 7; D1, n = 12; D2, n = 9; D1 + D1/D2, n = 6; D2 + D1/D2, n = 5). Control mice correspond to D1^{FlpO}/A2a^{Cre} mice injected with INTRSECT viruses transfecting cells with **C**on**F**on-eYFP construct (D1/D2^{eYFP}).

Extended Data Figure 4. Architecture of motor states and locomotion velocity during optogenetic stimulation. a-c, Effect of optogenetic stimulation motor architecture during locomotion (**a**), small movement (**b**), and immobility (**c**) quantified by the proportion of time spent in each state (left panels), bouts frequency (middle panels), and the average episode duration (right panels) in D1/D2, control D1/D2^{eYFP}, D1, D1 + D1/D2, D2, and D2 + D1/D2 mice (pre vs. light ON: *p < 0.05, **p < 0.01, ***p < 0.001). **d**, Averaged temporal evolution of mice velocity around locomotion onset during baseline ('Pre', left), during stimulation trials ('ON', middle left), between stimulation trials ('OFF', middle right), and difference observed in comparison with D1/D2 mice (right). **e**, Effect of laser illumination on average velocity (black) and top velocity (9th decile, green) during locomotion (pre vs. light ON: *p < 0.05, **p < 0.01, ***p < 0.001). **f**, Averaged temporal evolution of mice body center acceleration around locomotion onset during baseline ('Pre', left), laser illumination ('ON', middle left), between stimulation trials ('OFF', middle right), and difference in acceleration observed in comparison with D1/D2 mice (right). For all graphs: D1/D2, n = 13; control D1/D2^{eYFP}, n = 7; D1, n = 11; D1 + D1/D2, n = 6; D2, n = 8; and D2 + D1/D2, n = 5.

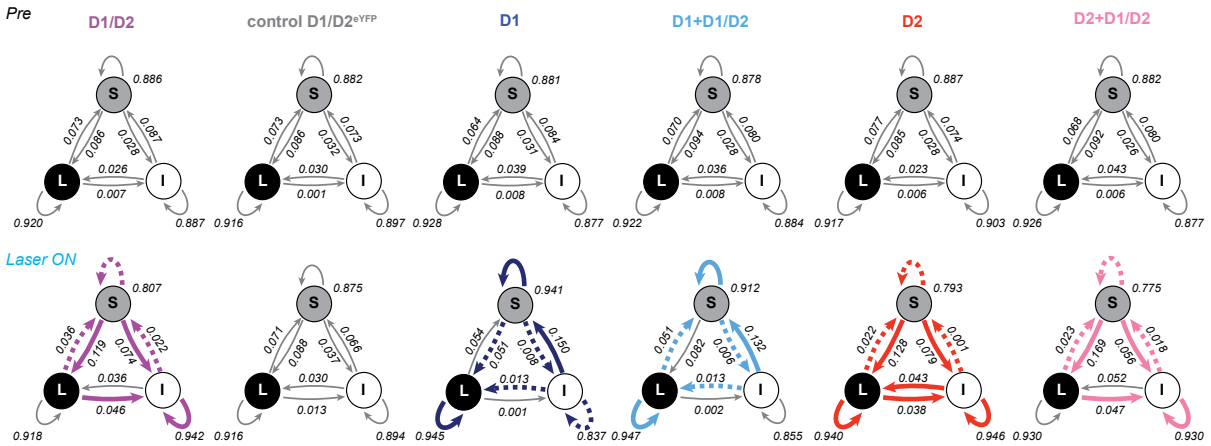

Extended Data Figure 5. Temporal organization of motor states. Representation of transition probabilities between the three motor states during baseline (top) and during laser illumination (bottom) of D1/D2-SPNs (n = 13 mice), control D1/D2^{eYFP}-SPNs (n = 7 mice), D1-SPNs (n = 11 mice), D2-SPNs (n = 8 mice), D1+D1/D2-SPNs (n = 6 mice) and D2+D1/D2-SPNs (n = 5 mice). Average transition probabilities are displayed next to corresponding arrow and arrows width reflects probabilities magnitude. For Laser ON condition, colored arrows indicate significant increases (solid lines) or decreases (dashed lines) in transition probabilities in comparison with baseline condition.

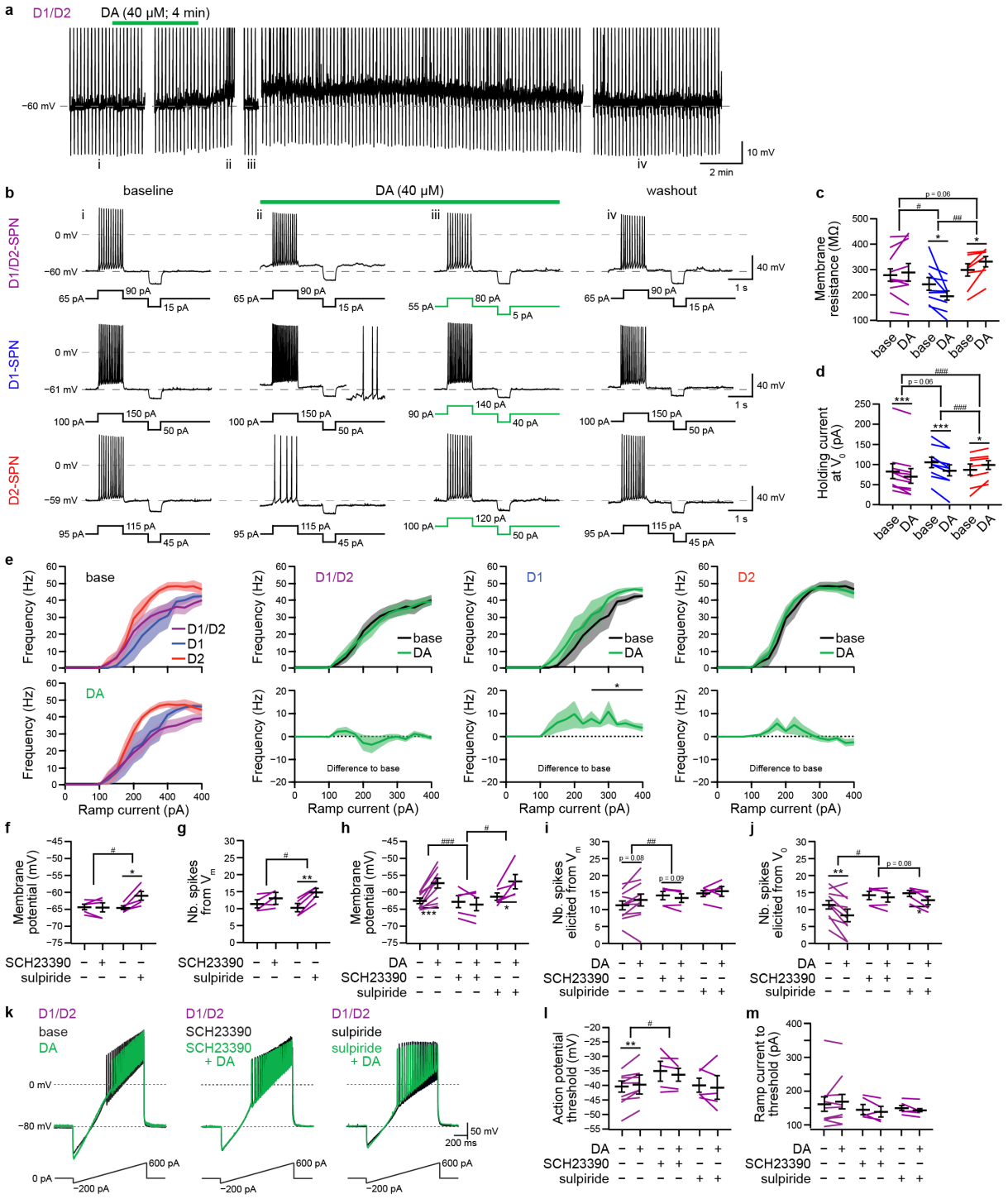

Extended Data Figure 6. Effects of DA application on SPNs subpopulations. a, Representative example of the effect of bath applied DA (40 µM, 4 min) on membrane potential and evoked firing activity in one D1/D2-SPN. **b**, Voltage traces recorded in one representative D1/D2-SPN (top), one D1-SPN (middle), and one D2-SPN (bottom) in response to depolarizing and hyperpolarizing current steps during baseline (first column), at peak of DA effect from the same holding current than in the beginning of the recording (second column), at peak of DA from holding current to restore voltage at the start of the recording (third column), and after DA washout (last column). For the D1/D2-SPN example i-iv represent times indicated in **a**. **c-d**, Quantification of changes in membrane resistance (around –60 mV) induced by DA application (**c**), and change in holding necessary to maintain cells at the same potential than at the begging of the recording before and after DA application (**d**) in D1/D2 (n = 10, violet), D1- (n = 9, blue), and D2-SPNs (n = 7, red) and (paired t-tests between baseline and after DA application: *p < 0.05, **p < 0.01, ***p < 0.001; t-tests comparing the magnitude of DA effect between SPN subpopulations: #p < 0.05,

$^{\#\#}p < 0.01$, $^{\#\#\#}p < 0.001$). **e**, Changes in average current-frequency relationship evaluated from ramp current injection during baseline and at the peak of DA effect in D1/D2- (n = 11), D1- (n = 6), and D2-SPNs (n = 8) and (paired t-tests between baseline and after DA application: $^{*}p < 0.05$). **f-g**, Effect of D1R antagonist (SCH23390, 10 µM) and D2R antagonist (sulpiride, 10 µM) application on membrane potential (**f**) and number of spikes elicited by a depolarizing current step (**g**) in D1/D2-SPNs (SCH23390, n = 5; sulpiride, n = 5) (paired t-tests between baseline and after antagonist application: $^{*}p < 0.05$, $^{**}p < 0.01$; t-tests comparing the magnitude of effect between treatments: # $p < 0.05$). **h-j**, Effect of DA application on D1/D2-SPNs without any pre-treatment, in the presence of SCH23390, or in the presence of sulpiride on the membrane potential (**h**), the number of elicited spiked by a depolarizing pulse from current membrane potential (**i**), and the number of spikes elicited from initial membrane potential (**j**) (no treatment, n = 11; SCH23390, n = 5; sulpiride, n = 5) (paired t-tests between baseline and after DA application: $^{*}p < 0.05$, $^{**}p < 0.01$, $^{***}p < 0.001$; t-tests comparing the magnitude of DA effect between treatments: $^{\#}p < 0.05$, $^{\#\#}p < 0.01$, $^{\#\#\#}p < 0.001$). **k**, Voltage response and APs of representative D1/D2-SPNs to ramp current injection before (black) and after (green) DA application without pre-treatment (left), in the presence of SCH23390 (middle), or in the presence of sulpiride (right). **l-m**, Effect of DA application on AP threshold (**l**) and minimal ramp current to elicit discharge (**m**) in D1/D2-SPNs without antagonists (n = 10), or in the presence of SCH23390 (n = 5), or sulpiride (n = 5) (paired t-tests between baseline and after DA application: $^{*}p < 0.05$, $^{**}p < 0.01$; t-tests comparing the magnitude of DA effect between conditions: $^{\#}p < 0.05$).

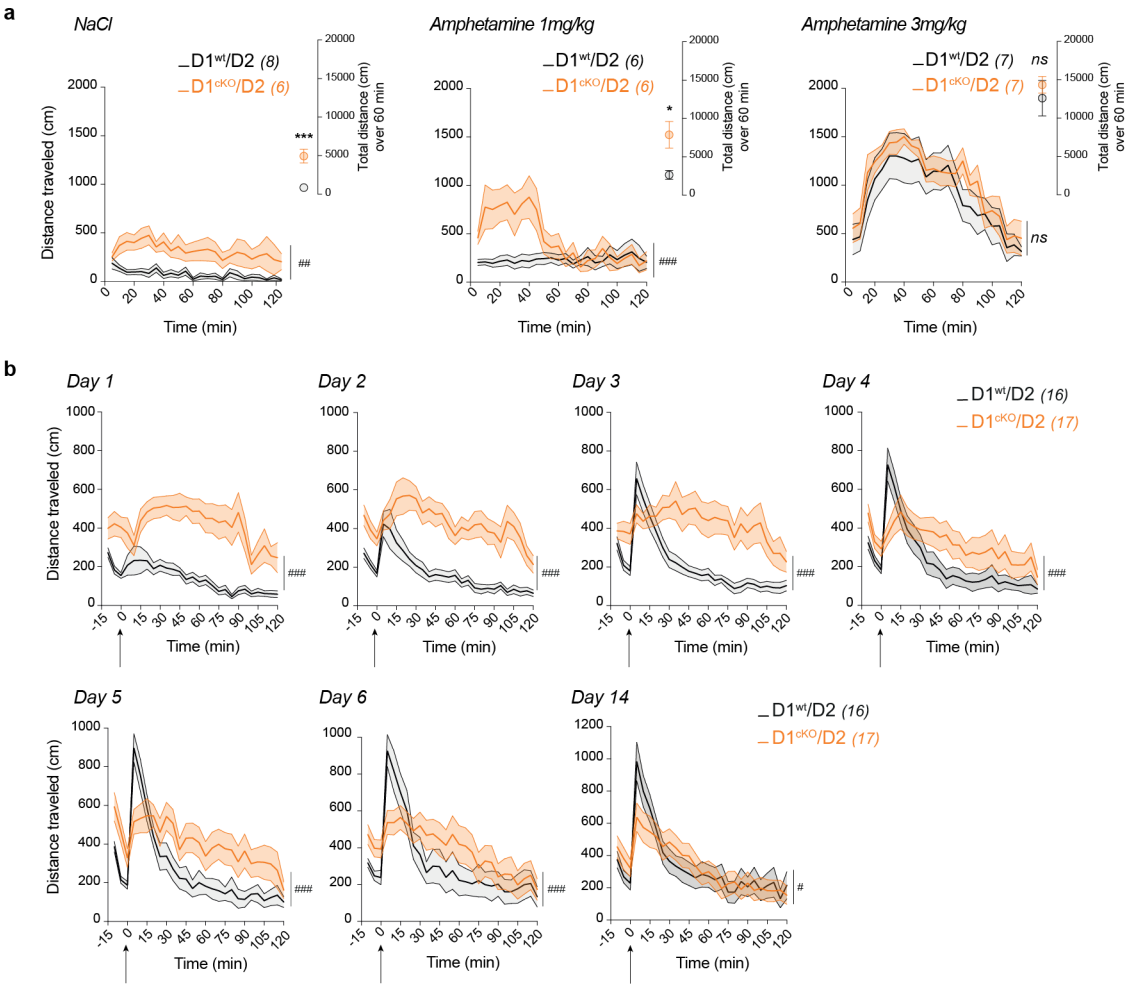

Extended Data Figure 7. Supplements on the phenotypic characterization of D1^{cKO}/D2 mice. a, Temporal distribution of the locomotor effects of acute amphetamine or saline injections in D1^{wt}/D2 and D1^{cKO}/D2 mice and (inserts) total distance travelled over the first 60 min after injection (D1^{wt}/D2 vs. D1^{cKO}/D2 mice: *p <0.05, **p < 0.01, ***p < 0.001). **b**, Temporal evolution of traveled distance across repeated 10 mg/kg cocaine injection in D1^{wt}/D2 (black) and D1^{cKO}/D2 mice (orange) (D1^{wt}/D2 vs. D1^{cKO}/D2 mice: *p <0.05, **p < 0.01, ***p < 0.001).

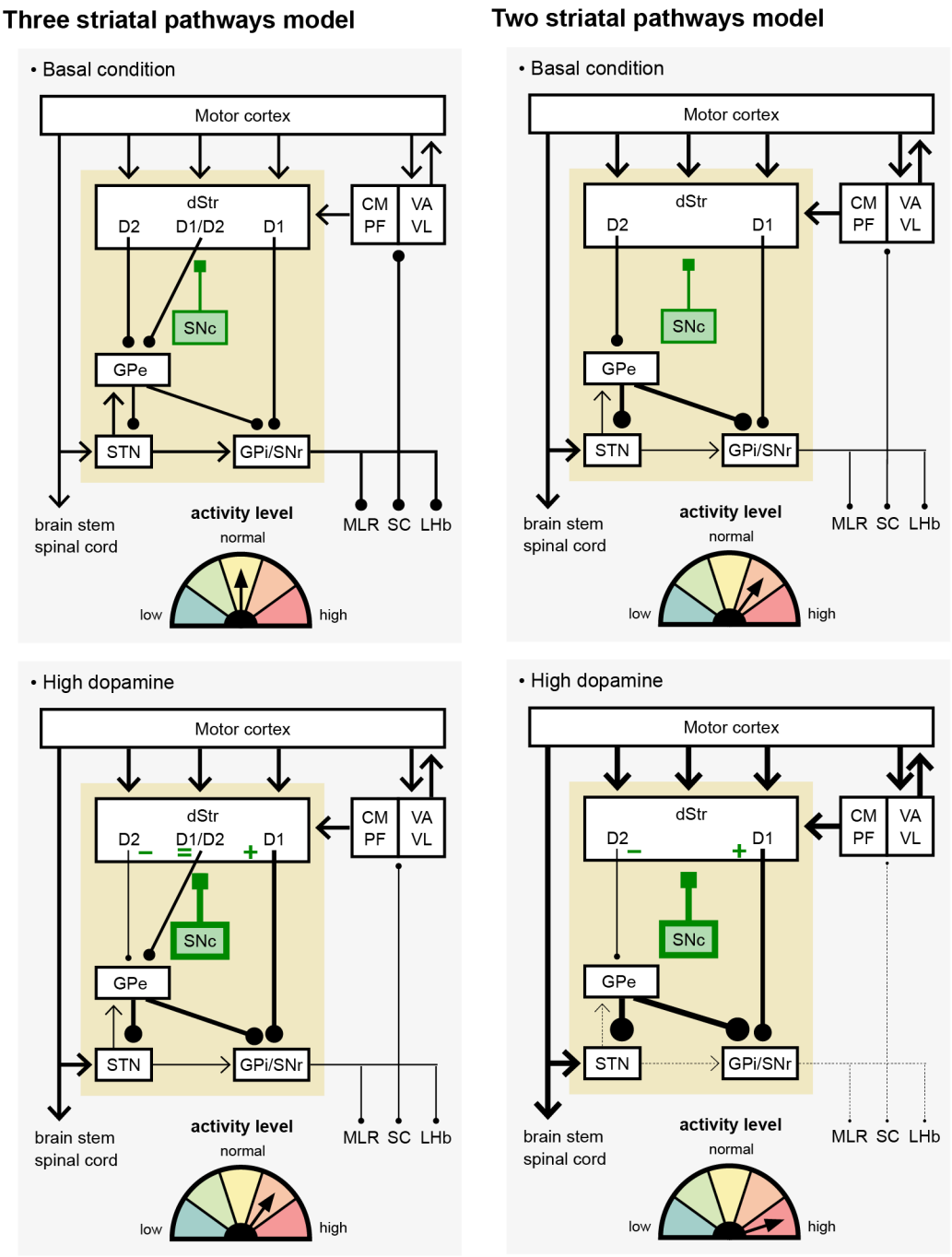

Extended Data Figure 8. Proposed model of integration of D1/D2-SPNs into striatal physiology. Updated model of the dorsal striatum control over motor states. We propose that the inhibitory control of D1/D2-SPNs on the GPe provides a necessary balance –especially in the context of high dopaminergic influx– to overcome an overly strong inhibition of the basal ganglia output nuclei resulting in overactivation of thalamo-cortical systems and thus a potentially detrimental hyperlocomotion. Indeed, by adding the projection of D1/D2-SPNs into the GPe, the three-pathways model succeeds in explaining the differences observed between wild-type and $D1^{cKO}$/D2 mice mimicking striatal function when it contains the two direct and indirect output pathways classically described (two-pathways model). Moreover, when dopaminergic neurotransmission increases, the two-pathways model fails to provide sufficient inhibition on the GPe, which would lead to a cessation of in the STN and GPi/SNr. On the other hand, the remaining inhibitory drive on the GPe from D1/D2-SPNs in the three-pathways model preserves some moderate activity in the basal ganglia output nuclei, which protects against cortical overactivation and unsustainable locomotor activity. (*Abbreviations: dSTR: dorsal striatum; GPe, external segment of the globus pallidus; STN, subthalamic nucleus; GPi,internal segment of the globus pallidus ; SNr, substantia nigra pars reticulata; SNc, substantia nigra pars compacta; CM, central medial thalamic nucleus; PF, parafascicular thalamic nucleus; VA, ventral anterior thalamic nucleus; VL, ventrolateral thalamic nucleus; MLR, mesensephalic locomotor region; SC, superior colliculus; LHb, lateral habenula)*

Passive membrane properties	D1/D2 neurons n = 21	D1 neurons n = 14	D2 neurons n = 19
(1) Resting potential (mV) ANOVA: NS ($F_{2,51}$ = 2.02; p = 0.14)	−69.67 ± 0.77	−72.86 ± 1.49	−71.05 ± 1.13
(2) Input Resistance (MΩ) ANOVA: NS ($F_{2,51}$ = 0.83; p = 0.44)	110.13 ± 6.93	1 115.81 ± 16.75	29.94 ± 12.43
(3) Membrane time constant (ms) ANOVA: NS ($F_{2,51}$ = 2.55; p = 0.09)	6.48 ± 0.35	5.16 ± 0.48	6.02 ± 0.39
(4) Membrane capacitance (pF) ANOVA: NS ($F_{2,51}$ = 2.10; p = 0.13)	61.14 ± 3.40	49.70 ± 4.98	50.20 ± 3.58
(5) Sag index (%) ANOVA: NS ($F_{2,51}$ = 0.24; p = 0.79)	13.39 ± 1.02	12.04 ± 1.63	13.83 ± 1.12
Just above threshold properties	**D1/D2 neurons n = 21**	**D1 neurons n = 14**	**D2 neurons n = 19**
(6) Step intensity to first spike (pA) ANOVA: p = 0.014 ($F_{2,51}$ = 4.65)	123.33 ± 10.74 < D1	176.43 ± 19.66 > D1/D2 . D2	121.58 ± 11.68 < D1
(7) Latency to first spike (ms) ANOVA: NS ($F_{2,51}$ = 0.01; p = 0.99)	528.12 ± 53.15	516.11 ± 66.61	521.17 ± 49.89
(8) Action potential threshold (mV) ANOVA: p < 0.001 ($F_{2,51}$ = 15.03)	−41.39 ± 1.05 <<< D1 < D2	−31.46 ± 1.70 >>> D1/D2 >> D2	−37.15 ± 1.11 > D1/D2 << D1
(9) Adaptation (Hz/s) ANOVA: NS ($F_{2,51}$ = 0.58; p = 0.57)	4.46 ± 1.08	3.06 ± 0.87	3.67 ± 0.61
(10) Minimal steady state frequency (Hz) ANOVA: NS ($F_{2,51}$ = 2.00; p = 0.15)	6.96 ± 0.46	8.25 ± 0.64	8.12 ± 0.49
Firing properties	**D1/D2 neurons n = 21**	**D1 neurons n = 14**	**D2 neurons n = 19**
(11) Early slope of current-frequency curve (Hz/pA) ANOVA: p < 0.001 ($F_{2,51}$ = 1.55)	0.20 ± 0.01 < D2	0.17 ± 0.01 <<< D2	0.25 ± 0.02 >>> D1 >> D1/D2
(12) Intensity to saturation (pA) ANOVA: p < 0.001 ($F_{2,51}$ = 9.00)	666.67 ± 49.80 >> D2	717.86 ± 46.77 >>> D2	470.00 ± 27.98 <<< D1 << D1/D2
(13) Amplitude of early frequency adaptation (Hz) ANOVA: NS ($F_{2,51}$ = 0.83; p = 0.44)	34.56 ± 3.15	27.85 ± 4.33	28.64 ± 4.83
(14) Time constant of early frequency adaptation (ms) ANOVA: p = 0.006 ($F_{2,51}$ = 5.60)	42.23 ± 4.34 < D2	54.97 ± 8.10	67.53 ± 5.20 >> D1/D2
(15) Slope of late adaptation (Hz/s) ANOVA: NS ($F_{2,51}$ = 1.66; p = 0.20)	−14.09 ± 1.14	−18.20 ± 2.47	−14.37 ± 1.60
(16) Maximal steady state frequency (Hz) ANOVA: NS ($F_{2,51}$ = 0.75; p = 0.48)	40.95 ± 2.07	43.81 ± 1.57	39.86 ± 2.53
(17) Spike frequency adaptation (%) ANOVA: NS ($F_{2,51}$ = 1.34; p = 0.27)	97.70 ± 5.06	92.45 ± 3.68	104.64 ± 5.50
Action potentials properties	**D1/D2 neurons n = 21**	**D1 neurons n = 14**	**D2 neurons n = 19**
(18) First spike amplitude (mV) ANOVA: p < 0.001 ($F_{2,51}$ = 10.74)	95.12 ± 1.29 >>> D1 >> D2	84.03 ± 2.52 <<< D1/D2	87.14 ± 1.68 < D1/D2
(19) Second spike amplitude (mV) ANOVA: p = 0.049 ($F_{2,51}$ = 3.08)	85.87 ± 1.68 > D1	79.46 ± 1.76 < D1/D2	82.87 ± 1.82
(20) First spike duration (ms) ANOVA: p < 0.001 ($F_{2,51}$ = 12.75)	3.01 ± 0.15 >>> D2 >> D1	2.46 ± 0.09 < D1/D2	2.22 ± 0.08 <<< D1/D2
(21) Second spike duration (ms) ANOVA: p < 0.001 ($F_{2,51}$ = 10.14)	3.36 ± 0.17 >>> D2 > D1	2.81 ± 0.09 < D1/D2	2.57 ± 0.10 <<< D1/D2
(22) First spike half-width (ms) ANOVA: p < 0.001 ($F_{2,51}$ = 13.36)	1.71 ± 0.09 >>> D2 >> D1	1.38 ± 0.05 < D1/D2	1.40 ± 0.06 <<< D1/D2
(23) Second spike half-width (ms) ANOVA: p < 0.001 ($F_{2,51}$ = 9.94)	1.87 ± 0.10 >>> D2 > D1	1.55 ± 0.05 < D1/D2	1.40 ± 0.06 <<< D1/D2
(24) First spike AHP (mV) ANOVA: p < 0.001 ($F_{2,51}$ = 10.37)	−11.03 ± 0.91 >>> D2 > D1	−14.51 ± 1.04 < D1/D2	−16.77 ± 0.89 <<< D1/D2
(25) Second spike AHP (mV) ANOVA: NS ($F_{2,51}$ = 0.931; p = 0.40)	−14.35 ± 0.89	−15.28 ± 1.10	−16.01 ± 0.77
(26) First spike AHP latency (ms) ANOVA: p < 0.001 ($F_{2,51}$ = 8.38)	5.48 ± 0.26 >>> D2 > D1	4.67 ± 0.20 < D1/D2	4.29 ± 0.15 <<< D1/D2
(27) Second spike AHP latency (ms) ANOVA: p = 0.002 ($F_{2,51}$ = 6.93)	8.44 ± 0.69 >> D2 > D1	5.97 ± 0.35 < D1/D2	5.97 ± 0.43 < D1/D2
(28) Spike amplitude reduction (%) ANOVA: p = 0.034 ($F_{2,51}$ = 3.61)	9.66 ± 1.47 > D1 . D2	4.92 ± 1.99 < D1/D2	4.86 ± 1.13 < D1/D2
(29) Spike duration increase (%) ANOVA: NS ($F_{2,51}$ = 1.69; p = 0.20)	12.00 ± 1.27	14.71 ± 1.58	15.47 ± 1.59
(30) Spike half-width increase (%) ANOVA: NS ($F_{2,51}$ = 1.51; p = 0.23)	8.92 ± 1.62	13.06 ± 2.09	12.59 ± 2.00

Extended Data Table 1. Complete list of electrophysiological properties recorded in D1/D2-, D1- and D2-SPNs. n: number of cells; NS: nonsignificant.Tukey post hoc tests: <, <<, <<<: inferior with p < 0.05, p < 0.01, p < 0.001, respectively; >, >>, >>>: superior with p < 0.05, p < 0.01, p < 0.001, respectively.